공학박사 학위논문

A STUDY ON THE DEVELOPMENT OF
SURGICAL-OPERATION-BY-WIRE (SOBW)
FOR ADVANCED SURGICAL ROBOT SYSTEM

차세대 수술 로봇을 위한
전기신호식 수술 로봇 제어 시스템
개발 연구

2015 년 8 월

서울대학교 대학원
협동과정 바이오엔지니어링 전공
이 치 원

A STUDY ON THE DEVELOPMENT OF
SURGICAL-OPERATION-BY-WIRE (SOBW)
FOR ADVANCED SURGICAL ROBOT SYSTEM

차세대 수술 로봇을 위한 전기신호식 수술 로봇 제어 시스템 개발 연구

지도교수 김 성 완

이 논문을 공학박사 학위논문으로 제출함

2015 년 7 월

서울대학교 대학원
협동과정 바이오엔지니어링 전공
이 치 원

이치원의 공학박사 학위논문을 인준함

2015 년 6 월

위 원 장	김 희 찬	(인)
부위원장	김 성 완	(인)
위 원	김 현 회	(인)
위 원	김 유 단	(인)
위 원	최 재 순	(인)

Ph. D. Dissertation

A STUDY ON THE DEVELOPMENT OF SURGICAL-OPERATION-BY-WIRE (SOBW) FOR ADVANCED SURGICAL ROBOT SYSTEM

BY

CHIWON LEE

JULY 2015

INTERDISCIPLINARY PROGRAM IN BIOENGINEERING

THE GRADUATE SCHOOL

SEOUL NATIONAL UNIVERSITY

A STUDY ON THE DEVELOPMENT OF SURGICAL-OPERATION-BY-WIRE (SOBW) FOR ADVANCED SURGICAL ROBOT SYSTEM

BY

CHIWON LEE

INTERDISCIPLINARY PROGRAM IN BIOENGINEERING

THE GRADUATE SCHOOL

SEOUL NATIONAL UNIVERSITY

THIS DISSERTATION IS APPROVED FOR THE DEGREE OF DOCTOR OF PHILOSOPHY

JUNE 2015

DOCTORAL COMMITTEE:

Chairman	*Hee Chan Kim, Ph. D.*
Vice Chairman	*Sungwan Kim, Ph. D.*
Member	*Hyeon Hoe Kim, M. D.*
Member	*Youdan Kim, Ph. D.*
Member	*Jaesoon Choi, Ph. D.*

서울대학교총장 귀하

Abstract

A STUDY ON THE DEVELOPMENT OF SURGICAL-OPERATION-BY-WIRE (SOBW) FOR ADVANCED SURGICAL ROBOT SYSTEM

By

Chiwon Lee

Interdisciplinary Program in Bioengineering
The Graduate School
Seoul National University

Although Minimally Invasive Surgery (MIS) affords several advantages compared to conventional open surgery, robotic MIS systems still have many limitations. Non-uniform gripping force issue of the da Vinci laparoscopic surgical robot is propounded and reported by other research group. In this research, a specific experiment is conducted and it is identified that non-uniform gripping force is caused by the EndoWrist's mechanical strings. EndoWrist's gripping forces, posture angles, and transferred torque are measured by using Torque-Transfer-System (TTS). The mean measured gripping forces of three different EndoWrists for 27 different postures were very diverse. The EndoWrist exerted different gripping forces, with a minimum

of 1.84-times more and a maximum of 3.37-times more in specific posture even if the surgeon applied the same amount of force. To overcome the non-uniform gripping force, two solutions are proposed in this study.

Firstly, mathematical solution that could be implemented in the existing system is developed in terms of software. Preliminary model of an EndoWrist-Inner-Mechanism-Model (EIMM) is developed and validated with a real gripping force measurements. Using the posture angles as input and the gripping forces as output, the EIMM is constructed. Then, expected gripping force values obtained from EIMM are compared with actual measurements of da Vinci EndoWrist to validate the proposed model. The prediction errors are observed by 10.69 – 16.25% for three different EndoWrists. From EIMM, surgeons will be beneficial with the understandings of actual gripping force being applied to tissue. This is significantly important to prevent serious injury by maintaining a proper force to tissue. If gripping motion trigger combines with pressure sensors to sense the surgeon's intention, EIMM will be modeled for soft and firm gripping motion.

Secondly, a novel idea for surgical instrument & entire system, Surgical-Operation-By-Wire (SOBW), was developed in terms of hardware to fundamentally resolve the limitation. To enhace the DOF, 6-axis external arm is integrated. The surgical instrument's mean gripping force (after 1,000 repetitions) at a pressure of 0.3 MPa was measured to be 5.8 N. The master interface employs the Hands-On-Throttle-And-Stick (HOTAS) controller used in aerospace engineering. To develop an improved HOTAS (iHOTAS) controller, 6-axis force/torque sensor was integrated in the special housing. The

reaction time was found to be 0.2 s. To evaluate the system's clinical applicability, the simple peg task experiment and workspace simulation are performed with five novice volunteers using a Fundamentals of Laparoscopic Surgery (FLS) board kit. All novice volunteers could complete the simple peg task within a mean time of 176 s (cut-off time: 300 s). The system's workspace was calculated to be 11,157.0 cm^3.

Therefore, the proposed concept of SOBW is expected to be widely used because it could deliver the uniform gripping force to the tissue.

Keywords: Laparoscopic surgical robot, End-effector of surgical robot, Gripping force modeling, Surgical-operation-by-wire, Pneumatic gripper.

Student number: 2011-23432

List of Tables

List of Figures

Contents

1. Introduction

1.1. Robotic Laparoscopic Surgery

Minimally Invasive Surgery (MIS) using conventional laparoscopic tools has emerged as a new paradigm for surgical operation because it offers many advantages such as smaller incision, reduced hemorrhaging, less pain, reduced exposure of internal organs to possible external contaminants, faster recovery, and short-term hospitalization period compared to conventional open surgery. MIS is thus greatly beneficial to patients. However, it suffers from some disadvantages: only skilled surgeons can perform non-robotic surgery, surgeons are not provided with haptic feedback, surgeries take longer compared with open surgery, suturing is difficult, and the Degree of Freedom (DOF) of the end-effector is less sufficient to perform surgery [1-3]. Robotic laparoscopic surgery has thus been rapidly developed as a means to resolve the issues faced with open surgery and non-robotic surgery [3-6]. The strengths and limitations for both surgeries operated by human and robots are presented in Table 1.1 [7]. The advantages and disadvantages of conventional laparoscopic surgery versus robotic laparoscopic surgery are summarized in Table 1.2 [4].

Table 1.1 Strengths and limitations for surgeries performed by humans and robots [7]

	Humans	Robots
Strengths	- Strong hand-eye coordination - Dexterous (at human scale) - Flexible and adaptable - Can integrate extensive and diverse information - Able to use qualitative information - Good judgment - Easy to instruct and debrief	- Good geometric accuracy - Stable and untiring - Can be designed for a wide range of scales - May be sterilized - Resistant to radiation and infection - Can use diverse sensors (force, etc.) in control
Limitations	- Limited dexterity outside natural scale - Prone to tremor and fatigue - Limited geometric accuracy - Limited ability to use quantitative information - Limited sterility - Susceptible to radiation and infection	- Poor judgment - Limited dexterity and hand-eye coordination - Limited to relatively simple procedures - Expensive - Technology in flux

Table 1.2 Advantages and disadvantages of conventional laparoscopic surgery versus robotics laparoscopic surgery [4]

	Conventional laparoscopic surgery	Robotic laparoscopic surgery
Advantages	- Well-developed technology - Affordable and ubiquitous - Proven efficacy	- 3-D visualization - Improved dexterity - High degrees of freedom - Elimination of fulcrum effect - Elimination of physiologic tremors - Ability to scale motions - Micro-anastomoses possible - Tele-surgery - Ergonomic position
Disadvantages	- Loss of touch sensation - Loss of 3-D visualization - Compromised dexterity - Limited degrees of motion - The fulcrum effect - Amplification of physiologic tremors	- Absence of touch sensation - Expensive - High start-up cost - May require extra staff to operate and big operating space

The usage of robots in surgical procedures is rapidly increasing because of many advantages by robotic laparoscopic surgery. The Puma 560 was the pioneer in robotic surgery operation; it was used in 1985 to operate neurosurgical biopsies with greater precision [4, 8]. Then, the first FDA approved surgical robot, ROBODOC was developed to perform a hip replacement surgery [9, 10]. The concept of tele-surgery using robotic technology was introduced by the National Air and Space Administration (NASA) and Stanford Research Institute (SRI) developed the dexterous tele-operated surgical robot in 1990s [9]. After the Automated Endoscopic System for Optimal Positioning (AESOP) robot was marketed, the Integrated Surgical Systems (the predecessor of Intuitive Surgical) licensed the SRI Green Telepresence Surgery system and developed the da Vinci laparoscopic surgical robot system [4, 11]. Also, the Zeus (Computer Motion Inc., Santa Barbara, CA, USA) surgical robot system was developed around the same time. However, Intuitive Surgical and Computer Motion merged into a single company. As a result, the Zeus system phased out in the early 2000s [12]. These surgical robot systems are presented in below Fig. 1.1 [13-15].

The market-leading surgical robotics system, the da Vinci (Intuitive Surgical, Inc., Sunnyvale, CA, USA) as shown in Fig. 1.2-(a), has demonstrated its safety and efficacy in laparoscopic surgery. This robot did not performed itself and its movements were controlled by skillful surgeon. Surgeon controlled master interface in work-console, then patient side manipulator and EndoWrist mimicked the movements of the surgeon’s motion. The number of operations

performed with the da Vinci rapidly increases every year [16]. Over the last decade, more than 1.5 million laparoscopic surgical operations, including gynecologic, cardiac, urology, thoracic, head & neck, and general surgery, have been performed worldwide using the da Vinci robot [16]. Since its launch, da Vinci robot has greatly reduced the number of open surgeries for common operation such as hysterectomy and prostatectomy [16, 17].

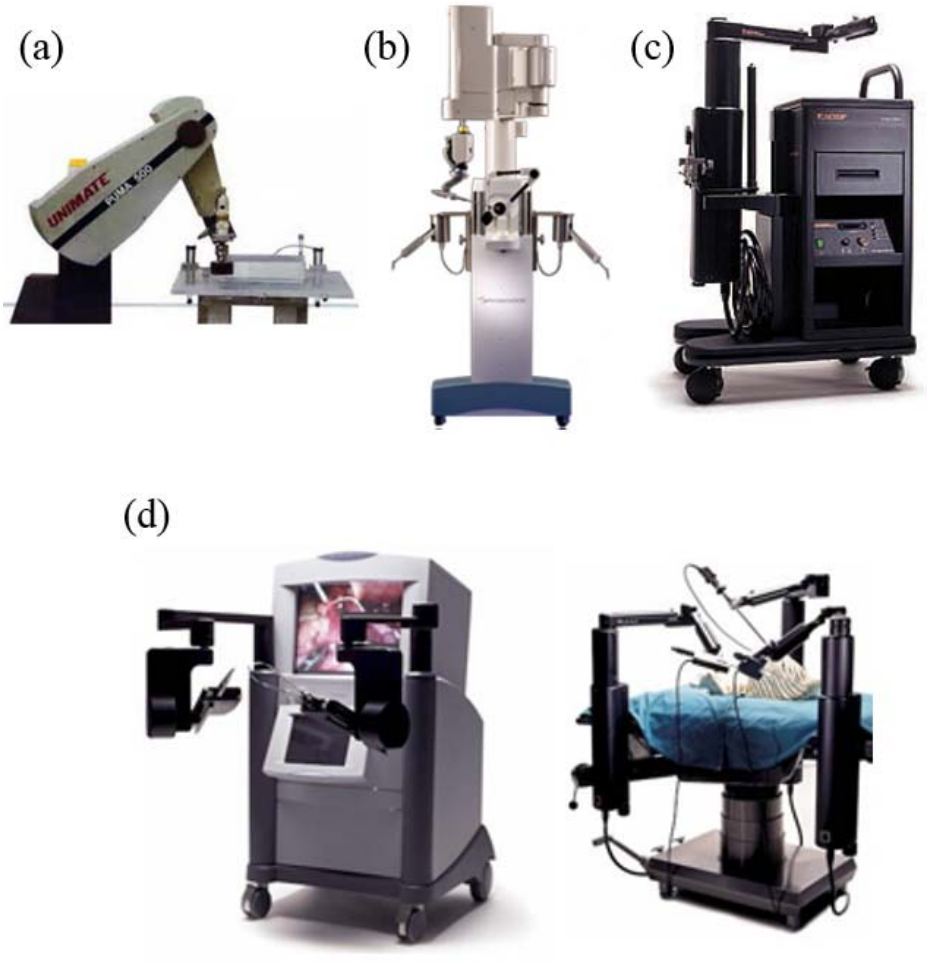

Fig. 1.1 (a) The Puma 560 [13]. (b) The ROBODOC [13]. (c) The Automated Endoscopic System for Optimal Positioning (AESOP) robot [14]. (d) The Zeus surgical robot system [15].

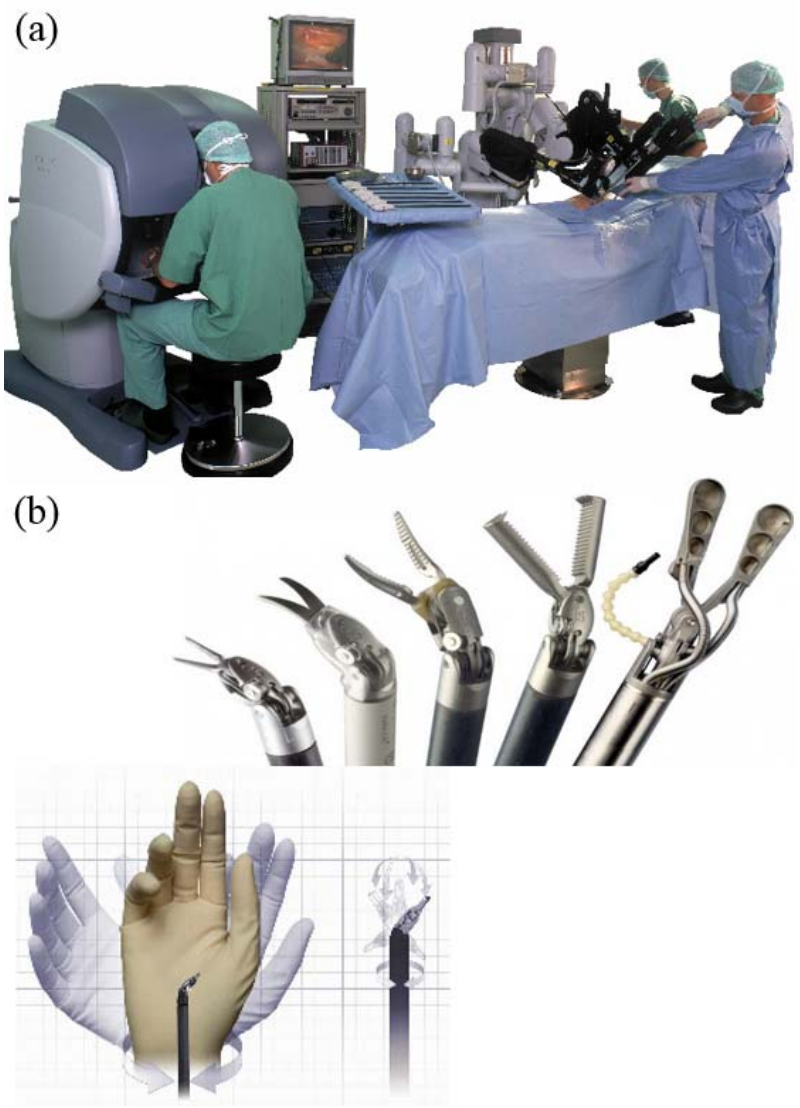

Fig. 1.2 (a) The da Vinci surgical robot system [18]. (b) The da Vinci surgical robot system's end-effectors, EndoWrists [19]. EndoWrists are designed to imitate the surgeon's dexterous hand motion.

1.2. End-effectors and Master Interfaces in Robotic Laparoscopic Surgery

One reason that da Vinci system has been able to successfully perform a wide range of surgeries is its unique design of end-effectors, EndoWrists, which are designed to allow surgeons to easily control the robot's movements [20] as shown in Fig. 1.2-(b). In the EndoWrist, four strings are connected to each servo motor in robot arm of the da Vinci; a surgeon's delicate hand movements can be reproduced inside the human body while minimizing the diameters of the opening ports.

However, in the current image-guided system for the da Vinci robot system, which has no haptic technology and no feedback on the gripping forces, a wide range of different gripping forces are observed with respect to the various postures of EndoWrist [21]. During the robotic surgery, surgeons do not realize that varying forces are being applied to the end-effector, because the system is an image-guided system; therefore, excessive mechanical force could be applied to cause the breakage of end-effector string (Fig. 1.3) or could cause serious tissue injury, such as cutting arteries or nerves [22-25].

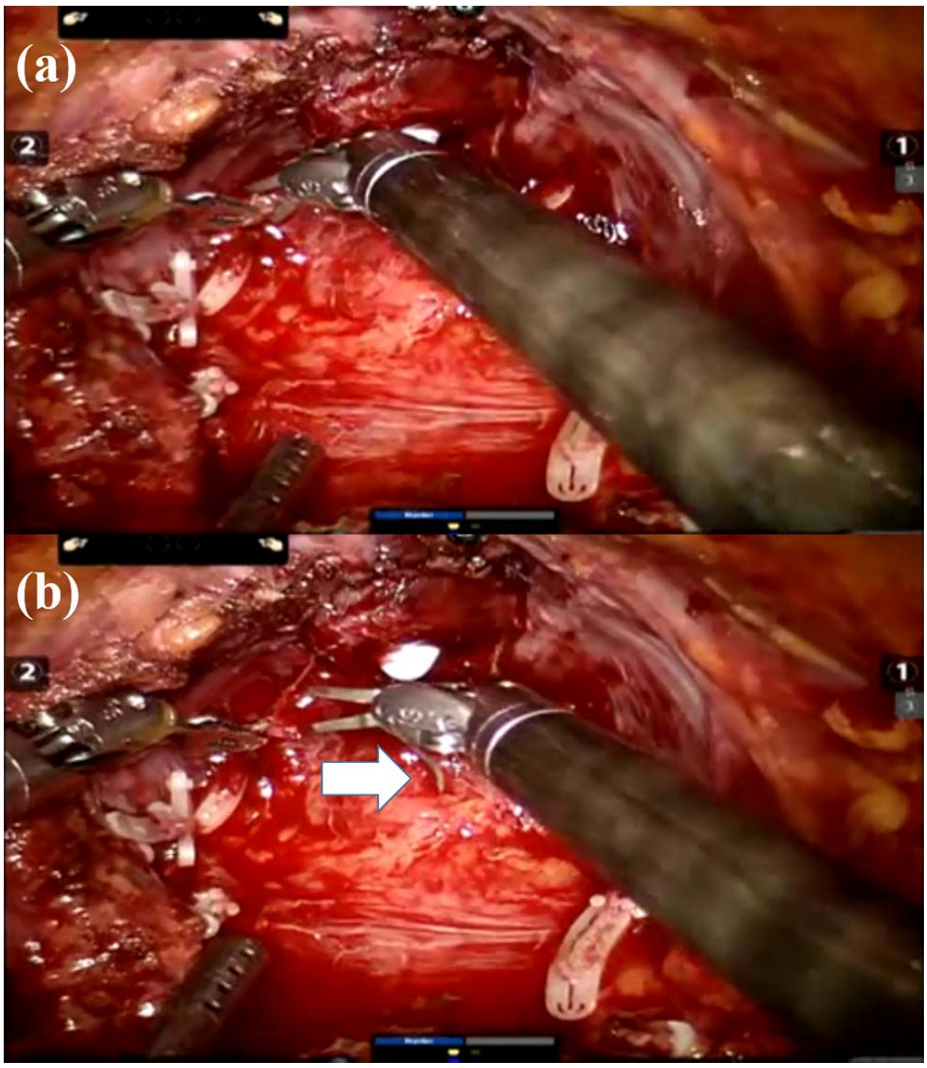

Fig. 1.3 (a) The small clip applier was bent to ligate the small artery (normal state). (b) The small clip applier suddenly became loose because of a broken string (failure state).

Many research groups have aimed to improve the surgical robot's end-effector system or to propose novel surgical robot systems. A surgical robot end-effector with a new joint mechanism for large force, accurate motion, and preventing joint hysteresis has been proposed [26]. Raven-II, a platform for collaborative research on advances in laparoscopic surgery, has been reported; this system has a 2-DOF spherical positioning mechanism and a 4-DOF instrument using mechanical strings [5]. A surgical intervention end-effector with integrated stereo vision has been developed [27]; this system's end-effector is inserted through a single 15 mm access port, and the end-effector's actuation unit is bulky. A single port laparoscopic robot where grippers and elbow/shoulder are decoupled has been developed [28]. This system is well integrated with decoupled joints and actuated for complex movement. However, one drawback of this system is the bigger diameter (18 mm) which needs to be reduced for small incision, too. These research groups have aimed to imitate users' wrist motions, such as pitching, yawing, rolling, and gripping motions, within an approximately 8 mm diameter as same diameter of da Vinci's EndoWrist. However, their proposed devices suffer from several drawbacks, including long peg task time, coupling with several moving joints, and bulky size [5, 26-28]. A gear driven mechanism is a general method being applied to conventional robot system, but it is very hard to be directly applicable to surgical robot end-effector system which has 8 - 10 mm of diameter. Some efforts using a gear system are found in [28], but the diameter is bigger than the above range. So, da Vinci system is a representative surgical robot system, but it is using mechanical string & pulley to keep the diameter within 8 mm and to sterilize.

To operate patient side manipulator, a surgeon sits at a work-console for manipulation of the master interface. Although enormous advances of master interface have been achieved in engineering aspect, limitations still exist. For instance, many master interfaces have restricted DOF. Many research groups have been developed various master interfaces to overcome limited DOF. The MASTER, a nine DOF finger-cuff type tele-manipulator that is similar to the da Vinci's master interface, is proposed from Nanyang Technological University [29]. The MiroSurge system's master interface closely mimics the da Vinci and has torque sensors in each joints [30, 31]. Pen-like controllers such as Phantom Omni and NeuroArm's master interface have been developed as well [5, 32, 33]. However, these master interfaces did not provide a proper force feedback and could not receive delicate force sensing from a surgeon.

1.3. Objectives and Scope

Securing sufficient gripping force is an important issue in a laparoscopic surgical robot system. However, the variation in forces according to the EndoWrist's postures is caused by the current end-effector's structure and design. In this research, different gripping forces for different postures are proven by the experiment. For gripping force experiment and new end-effector, four versions of the surgical robot end-effectors were developed. These end-effectors were named as a KS series (1-4). The first version of prototype, KS-1 was developed for analysis of existing surgical robot end-effector, EndoWrist. Design of the KS-1 was slightly large due to several mechanical parts (bearing, timing pulley, timing belt, coupling, etc.) as shown in Fig. 1.4. The KS-2, an improved version of the KS-1, was developed as a compact size as shown in Fig. 1.5. Eliminating many mechanical parts, KS-2 was directly driven by 4 servo motors and was used to measure the gripping force of the EndoWrist. This version could be attached to external arm and execute simple peg task. The KS-3 was a concept that replaces mechanical strings with electrical wires in the surgical robot system. However, KS-3 was not appropriate for the application of laparoscopic surgery since micro motor has small torque and relatively large diameter (14 mm) compared with EndoWrist (8 mm). A new concept of end-effector, KS-4, which was driven by pneumatic force and micro motor, was developed to secure sufficient gripping force, as described in section 2.2.3..

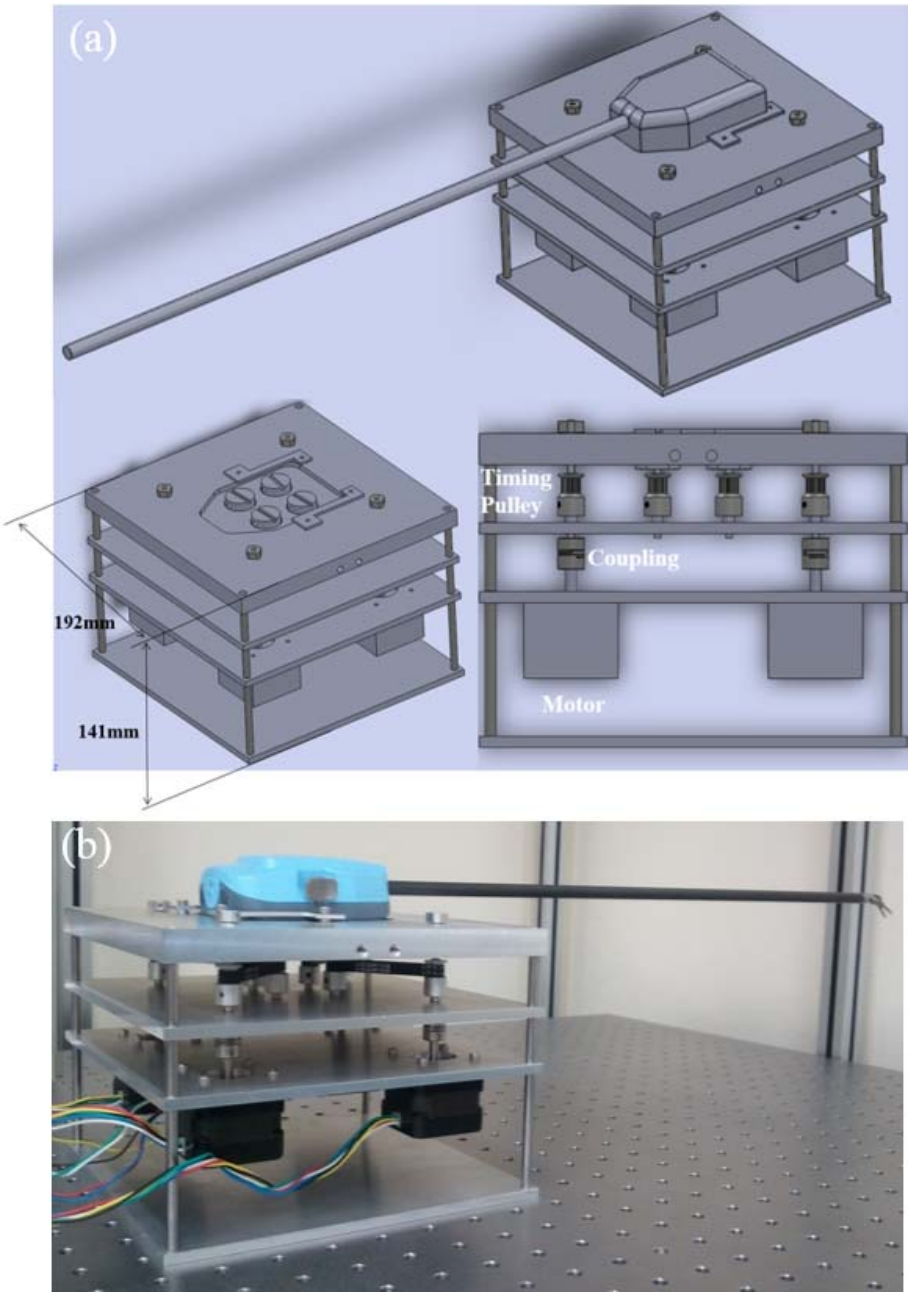

Fig. 1.4 Prototype version 1, KS-1. (a) 3-D design of KS-1. (b) In-house torque transfer mount and EndoWrist were assembled. The EndoWrist was driven by 4 step motors and several mechanical part (bearing, timing pulley, timing belt, coupling, etc.)

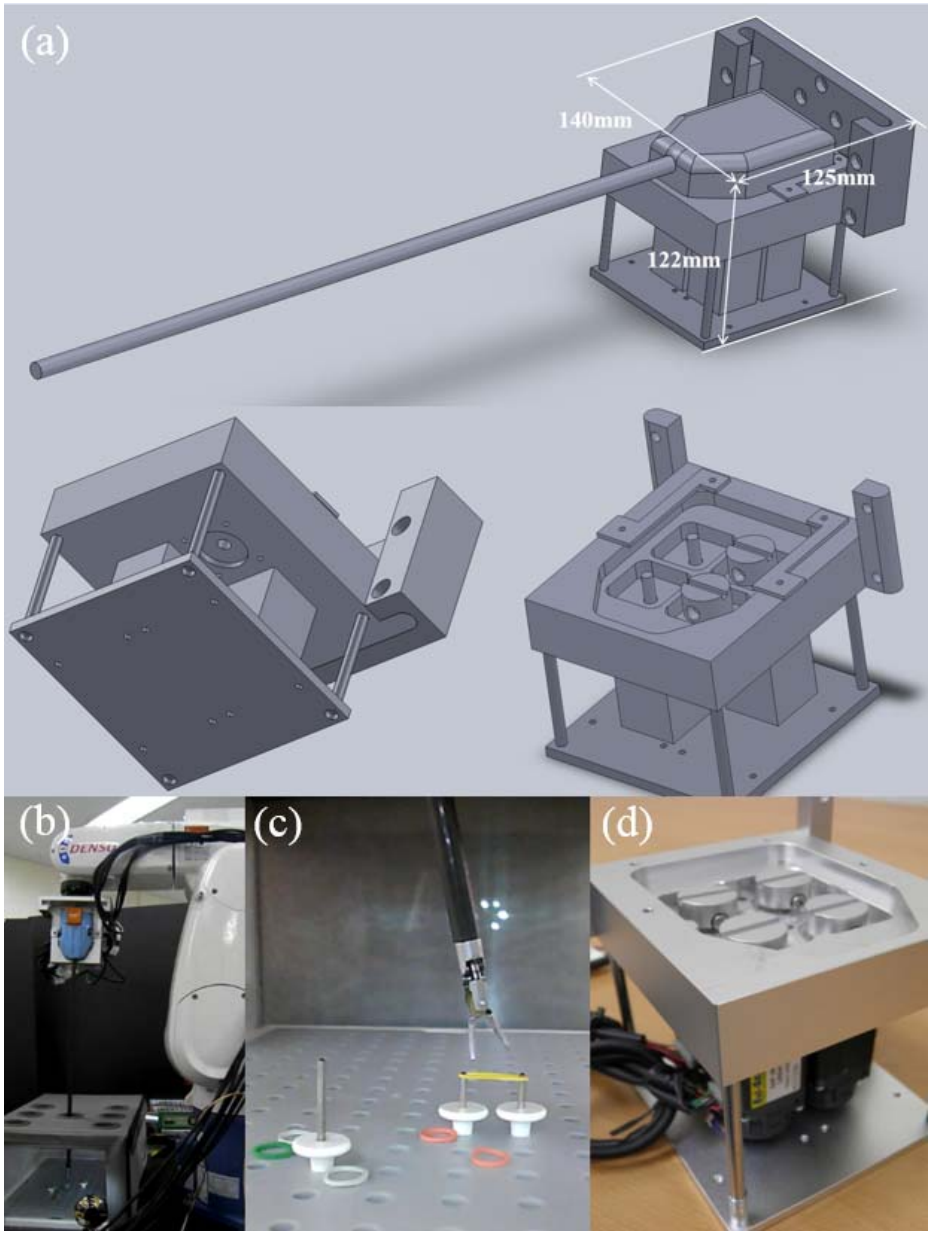

Fig. 1.5 Prototype version 2, KS-2. (a) 3-D design of KS-2. (b) External arm, in-house torque transfer mount (compact size), and EndoWrist were assembled. (c) Simple peg task using KS-2. (d) In-house torque transfer mount (compact size) for EndoWrist. The EndoWrist was driven by 4 servo motors, directly.

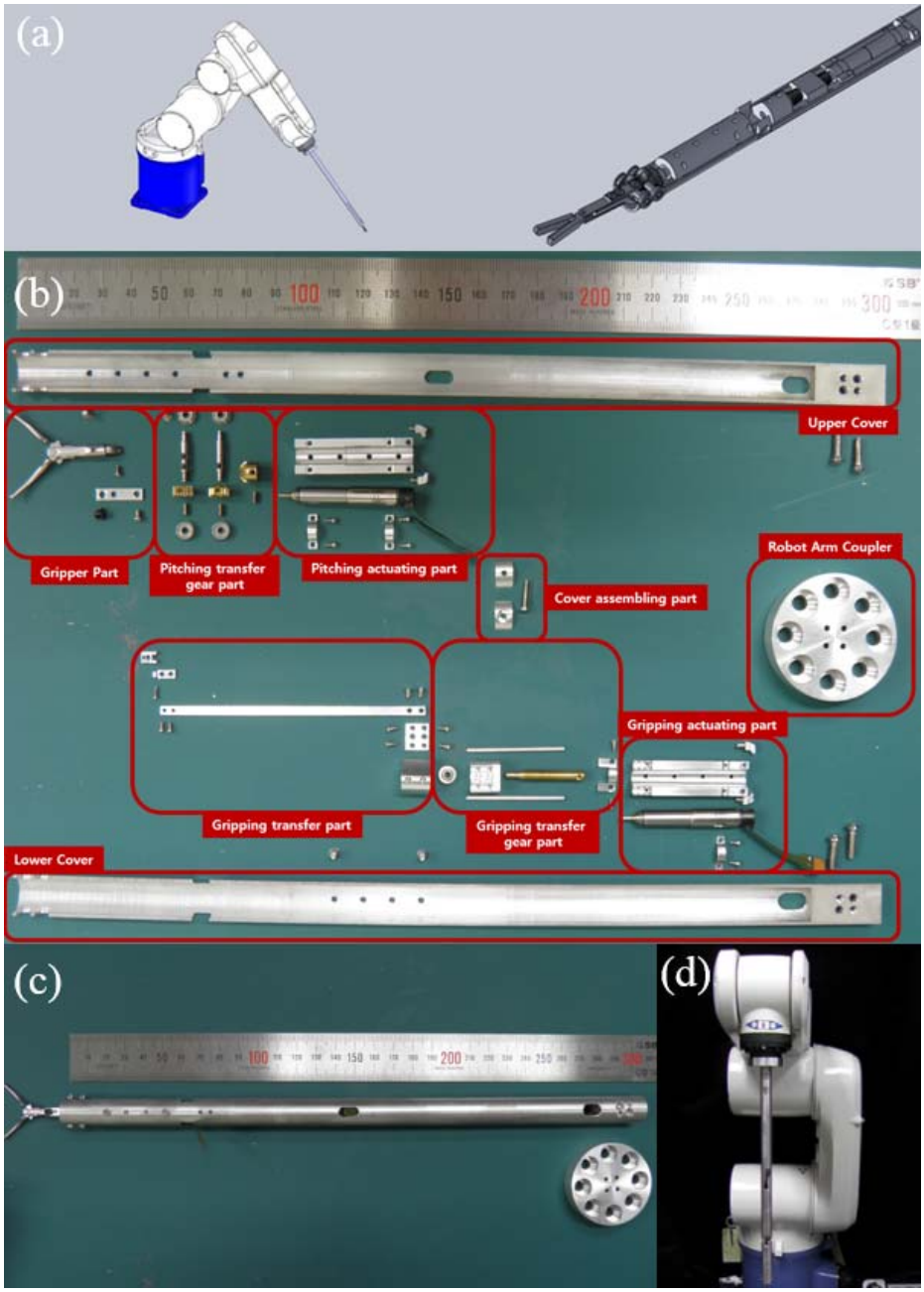

Fig. 1.6 Prototype version 3, KS-3. (a) 3-D design of KS-3. (b) Several mechanical and electrical parts. (c) Assembled KS-3. (d) KS-3 was attached to external arm. The KS-3 was driven by 2 micro motors (motor's diameter: 6 mm) for gripping motion and pitching motion.

To resolve a drawback of existing laparoscopic surgical robot's end-effector, two solutions are proposed in this research. Firstly, to predict the compensation gripping force, a mathematical model of EndoWrist's inner mechanism has been developed and validated by comparing the expected gripping force from the model with the measured gripping force from the da Vinci. These methodologies and results will be beneficial to improve the existing surgical robot systems for uniform gripping force with different postures. Secondly, pneumatic type of novel end-effector (KS-4) and surgical robot system are developed to solve the fundamental mechanical design problem. Furthermore, novel master interface is incorporated with surgical robot system for surgeon's stable, secure, and comfortable laparoscopic surgery.

1.3.1. Gripping Force Measurement for Various Postures and Mathematical Compensation Model

The torque or the force from the motor could not be transferred to the end-effector's gripper intact because of the friction and the interference among the four strings inside the end-effector [34]. To calculate the amount of gripping force that is required to compensate for an excessive or insufficient force, the relationship between the EndoWrist's position (posture) and the force transferred to the EndoWrist's gripper need to be determined; however, only limited and quantitative force difference was proven [21], and in-depth theoretical analyses of the excessive or insufficient force has not been previously conducted [35]. To prove the non-uniform gripping force problem, the EndoWrist's gripping forces, posture angles, and transferred torque are measured using the Torque Transfer System (TTS, KS-2's in-house torque transfer mount) which is proposed in this research.

1.3.1.1. Torque Transfer System (TTS)

A control block diagram for the EIMM is shown in Fig. 1.7. The input variable for the EIMM was the EndoWrist's posture angles ($\theta_1, \theta_2, \theta_3, \theta_4$), and the output variable was the EndoWrist's gripping force. Using the input and output variables, the unknown system of the EndoWrist's inner mechanism was identified using modeling techniques.

The da Vinci system used four servo motors to control the movement of the EndoWrist. To provide conditions similar to da Vinci's operation, the TTS (KS-2), which was composed of motors, connectors, an in-house mount kit, and a controller, was developed as depicted in Figs. 1.7 and 1.8. In the TTS, the four motors were the major torque power source. High-resolution, closed-loop controlled motors (Ezi-Servo-28L-D, Fastech, Bucheon City, GyeongGi-Do, Republic of Korea) were used to achieve a precision control for the EndoWrist.

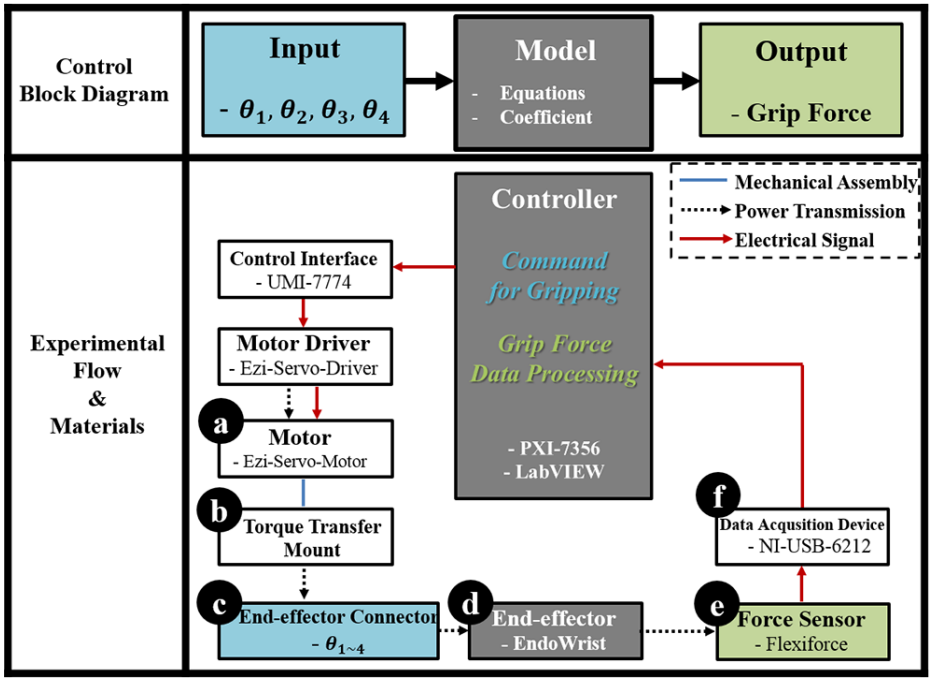

Fig. 1.7 Control block diagram and experimental flow for the Torque Transfer System (TTS). A da Vinci end-effector (EndoWrist) is mounted on the in-house torque transfer mount (b) and four motors (a) controlling the EndoWrist (d). Gripping forces are measured using a piezo-resistive sensor (e) through the specific electric circuit and data acquisition device (f) in accordance with the roll (α), pitch (β), and yaw (γ) movements of the EndoWrist.

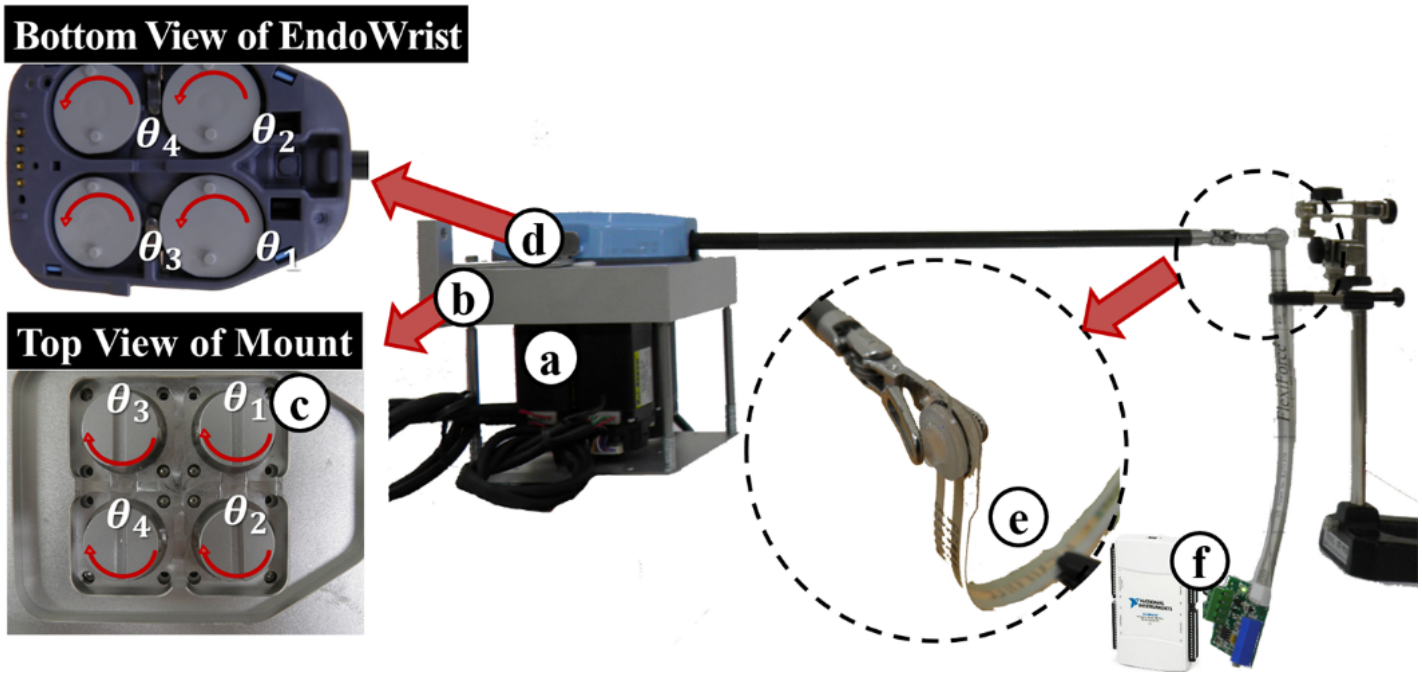

Fig. 1.8 Experimental set-up for the measurement of gripping forces inside the torque transfer mount. The parameters θ_1 and θ_2 are involved in the roll (α) and pitch (β) motions, respectively. The parameters θ_3 and θ_4 perform the yaw (γ) motion together.

A motor controller (PXI-7356 and UMI-7774, National Instruments (NI), Austin, TX, USA) and software (NI, LabVIEW) were used to control the motors.

The output variable of the gripping force was measured using a sensor that was placed between a pair of grippers, as shown in Fig. 1.8-(e). A flexible, piezo-resistive sensor (Flexiforce, Tekscan Inc., South Boston, MA, USA) was connected to a simple voltage-dividing circuit. Because the sensor changes its resistance according to the applied forces, the voltage across the sensor varied when the gripper grabs an object. For the acquisition of the signal, NI hardware (USB-6212) was used.

1.3.1.2. Calibration of the Sensors

A torque sensor (DynPick, Wacoh-Tech Inc., Takaoka City, Futatsuka, Japan) was connected to the EndoWrist's connectors, which were connected to the shaft of the motor. The transferred torque exerted from the motor on the EndoWrist was measured. The voltage reading of the torque sensor in accordance with the applied torque, and the linear relationship between the torque (T) and the voltage (output voltage of the torque sensor, V_T), was formulated as equation (1.1). Note that the DC offset could be eliminated by reading the sensor value (the mean calculated from 10 measurements: 0.2503

N·m, standard deviation: 0.0031 N·m) during the pre-load condition and the voltage coefficients were obtained from the sensor's datasheet.

$$T = \frac{V_T - 8192}{819} - 0.2503 \tag{1.1}$$

Using the equation (1.1), the torque was measured 10 times while the motor was fixed in place. The torque measurement of 0.0838 N·m (standard deviation: 0.0032 N·m) was exerted constantly from both sides of the gripper. This torque value was lower than the torque value for the da Vinci servo motor (RE25-118751, Value: 0.218 N·m, Maxon Motors, Brünigstrasse, Sachseln, Switzerland) [36, 37]. However, the measured gripping force (4.20 N ~ 20.33 N) was close to the da Vinci gripping force (5.52 N ~ 21.64 N) [21] because the da Vinci torque transfer system used string in da Vinci robot arm, which reduced the torque because of strings' interference, while the TTS was driven directly from the motor. Additionally, because the torque sensor was a 6-axis electrostatic capacitor type, the optimal experimental condition could be found using the sensor's results while the force (x, y, and z) and torque (x and y) were maintained at zero.

The linearity of the gripping force sensor was calibrated with metal weights. The voltage readings of the sensor (output voltage of the force sensor, V_F) were plotted against the varying metal weight numbers. All the measurements

were repeated 10 times, and their mean values were interpolated in equation (1.2) using a linear regression [38] as the sensor's datasheet. The standard deviation of the plotted data with equation (1.2) was 2.21%.

$$F = 11.3122 \times V_F - 3.0713 \tag{1.2}$$

1.3.1.3. Force Measurement with Respect to the EndoWrist's Posture

The analysis of the gripping force and its measurement were performed with three different EndoWrists; the Prograsp Forceps (P.F.), the PK Dissecting Forceps (P.D.F.), and the Large Needle Driver (L.N.D.). The input factors for controlling the EndoWrist were the angles of connectors ($\theta_1, \theta_2, \theta_3, \theta_4$) shown in the bottom view of EndoWrist (Fig. 1.8). The parameters θ_1 and θ_2 were involved in the roll (α) and pitch (β, proximal wrist joint movement) motions, respectively, as shown in Fig. 1.9-(a).

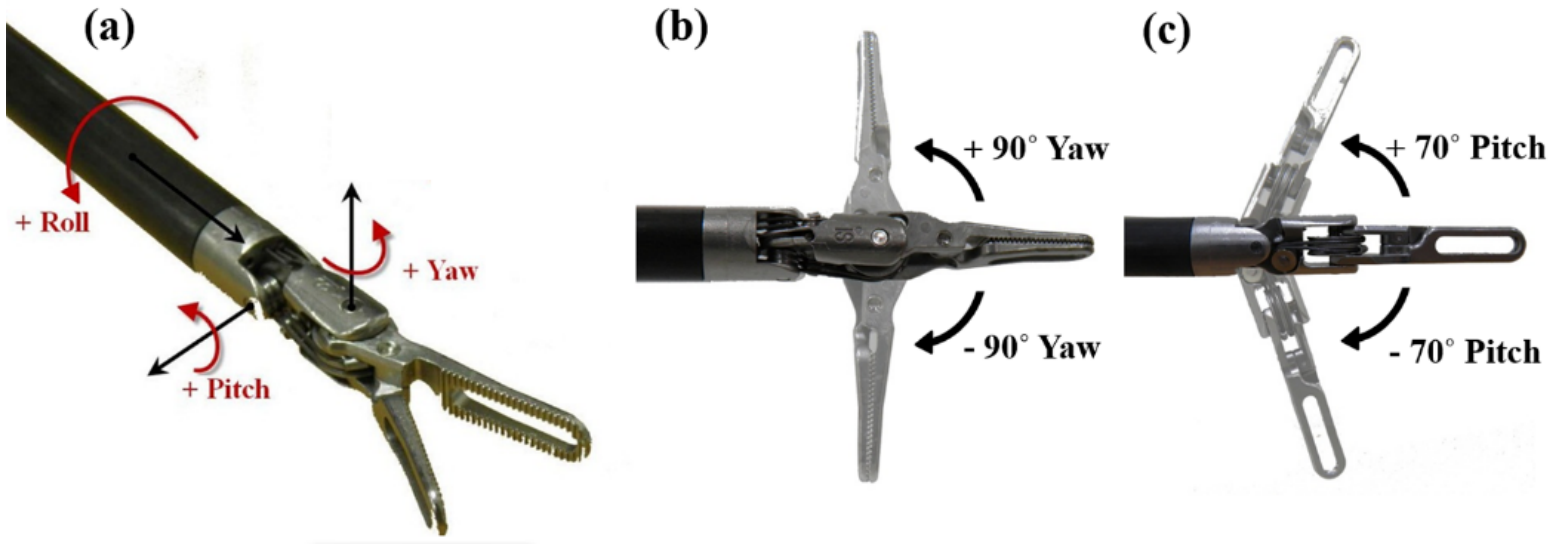

Fig. 1.9 The orientation of the EndoWrist. By moving the connectors (Fig. 1.8-(c)), the EndoWrist's orientation and posture are determined. (a) Isometric view. (b) Top view. (c) Side view. According to Fig. 1.9-(a), the EndoWrist's roll (α), pitch (β), and yaw (γ) orientations are located at different geometrical structures.

The parameters θ_3 and θ_4 performed the yaw (γ, distal wirst joint movement) motion together. When θ_3 and θ_4 move in the opposite direction, the end-effector's gripper operates open or closed. The relationship between the motor connector angle ($\theta_1, \theta_2, \theta_3, \theta_4$) and the Euler angle ($\alpha, \beta, \gamma$) was empirically calculated using equations (1.3), (1.4), and (1.5). However, in this research, because Euler angles were intuitive for surgeons, the roll (α), pitch (β), and yaw (γ) angles can be used instead of da Vinci EndoWrist's connector angle ($\theta_1, \theta_2, \theta_3, \theta_4$).

$$\theta_1 = -\frac{11}{18}\alpha \tag{1.3}$$

$$\theta_2 = -\frac{13}{14}\beta \tag{1.4}$$

$$\theta_{3,4} = \gamma - \frac{9}{14}\beta \tag{1.5}$$

The EndoWrist's roll (α), pitch (β), and yaw (γ) joints are located at different positions, as shown in Fig. 1.9-(a). A unique set of Euler angles gives a specific, fixed posture for the EndoWrist. The movement ranges of the Euler angle A(α, β, γ) in this case are -270°< α <270°, -70°< β <70°, and -90°< γ <90°,

respectively where A(α, β, γ) stands for the posture with Euler angle set (α, β, γ). For this research, the angles were selected separately using three steps for $\alpha, \beta,$ and γ whose values are (-90˚, 0˚, 90˚), (-70˚, 0˚, 70˚), and (-90˚, 0˚, 90˚), respectively. Therefore, a multiple analysis of variance ($3\times3\times3$) was used and Euler angle A(α, β, γ) was expressed as 27 postures of EndoWrist as shown in Table 1.3.

Table 1.3 Measured gripping forces for three different EndoWrists

Angle (Degree, ˚)			MGF (N) and SD (N)					
Roll	Pitch	Yaw	P.F.		P.D.F.		L.N.D.	
(α)	(β)	(γ)	MGF	SD	MGF	SD	MGF	SD
-90	-70	-90	12.12	0.20	5.34	0.14	11.68	0.15
		0	13.28	0.18	5.46	0.05	11.59	0.11
		90	17.28	0.35	4.93	0.06	10.33	0.48
	0	-90	16.68	0.77	4.62	0.04	12.95	0.22
		0	18.98	0.21	5.25	0.10	14.66	0.24
		90	14.35	0.35	6.83	0.09	11.69	0.27
	70	-90	19.15	0.40	5.28	0.03	11.79	0.18
		0	15.95	0.35	5.22	0.06	9.47	0.11
		90	11.58	0.40	4.20	0.08	9.00	0.11
0	-70	-90	11.62	0.26	10.64	0.23	16.14	1.21
		0	15.50	0.25	6.64	0.08	8.86	0.06
		90	17.73	0.22	6.16	0.09	10.48	0.22
	0	-90	20.33	0.31	7.33	0.07	12.00	0.12
		0	16.26	0.53	6.01	0.13	10.57	0.14
		90	15.41	0.54	8.08	0.24	11.67	0.40
	70	-90	11.05	0.21	11.5	0.10	15.12	0.34
		0	13.21	0.35	7.42	0.02	6.81	0.38
		90	13.63	0.36	6.72	0.18	12.52	0.58
90	-70	-90	14.94	0.27	9.26	0.11	11.41	0.12
		0	15.39	0.27	9.06	0.15	12.85	0.14
		90	14.92	0.46	6.25	0.14	7.17	0.09
	0	-90	17.02	0.51	12.10	0.08	9.89	0.26
		0	15.62	0.38	11.15	0.17	13.92	0.27
		90	14.86	0.34	12.18	0.48	11.99	0.16
	70	-90	13.94	0.23	14.15	0.28	17.73	0.38
		0	18.83	0.37	10.79	0.14	13.41	0.25
		90	13.51	0.25	10.02	0.28	8.82	0.21
Maximum Gripping Force			20.33		14.15		17.73	
Minimum Gripping Force			11.05		4.20		6.81	
Overall Mean of Gripping Force & SD			15.30	0.35	7.87	0.13	11.65	0.27
Cronbach's Alpha			0.99		1.00		0.99	
SEM			0.02		0.00		0.01	

* Abbreviation: Mean Gripping Force (MGF), Standard Deviation (SD), Standard Error of Measurement (SEM), Prograsp Forceps (P.F.), PK Dissecting Forceps (P.D.F.), and Large Needle Driver (L.N.D.).

The gripping force was measured 5 times for each combination which represents 27 postures. To understand the relationship between Euler angles and posture, four representative postures were illustrated as shown in Fig. 1.10.

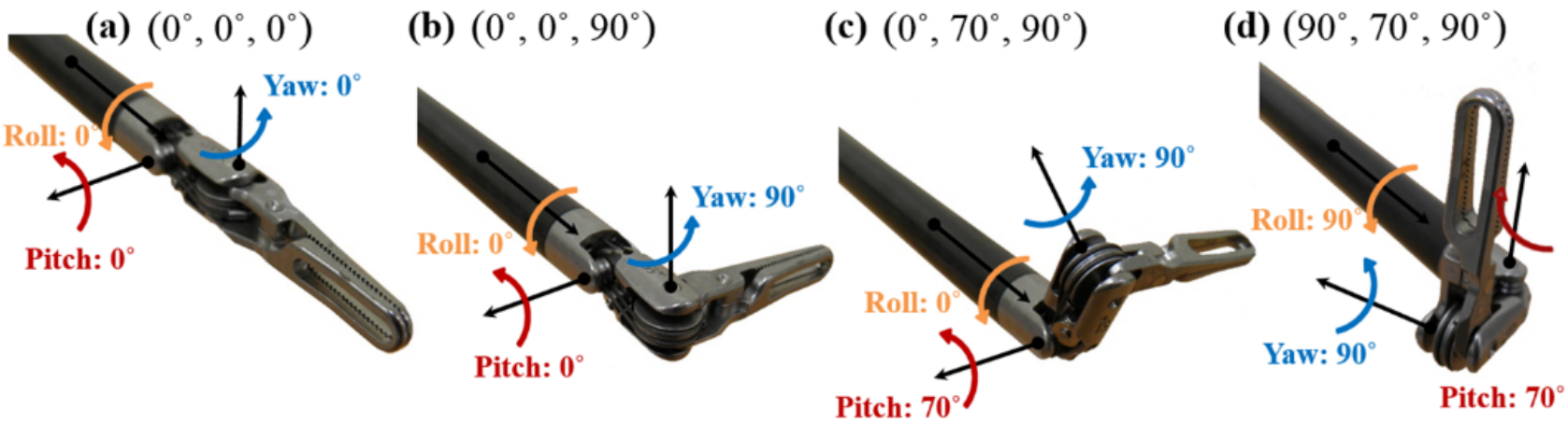

Fig. 1.10 The four representative posture at isometric view. (a) The posture for (0˚, 0˚, 0˚). (b) The posture for (0˚, 0˚, 90˚). (c) The posture for (0˚, 70˚, 90˚). (d) The posture for (90˚, 70˚, 90˚).

The consistency of measured gripping forces for three different EndoWrists was estimated using the Standard Error of Measurement (SEM) [39]. To estimate the SEM, the value of one subtract the reliability coefficient is taken, and the standard deviation of the experiments are multiplied by the square root of this value [40]. The SEM indicated measurement error with the same unit as the original measurement. A true difference between the measurement value and an error of measurement could be discriminated by SEM. To evaluate the consistency of 5 times of gripping force measurements for the 27 postures, Cronbach's alpha was used as the reliability coefficient for SEM among the several reliability definitions. The SPSS (IBM Corporation, Armonk, NY, US) was used for computing Cronbach's alpha [41]. The MATLAB software (The Mathwork, Inc., Natick, MA, USA, using Seoul National University Academic License) was used for calculating SEM.

In this research, the EndoWrist Inner Mechanism Model (EIMM) is developed to quantitatively and theoretically analyze the EndoWrist's gripping force. There are some differences between surgeon's control for the master interface of da Vinci system and our proposed automatic triggering method. The da Vinci robot's torque transfer mechanism to EndoWrist is different from our proposed TTS since the TTS is directly driven by 4 motors with minimal mechanical strings for allowing TTS to exert comparable gripping force with da Vinci system using only small capacity motor. However, since the surgeon's intention for the massive or tiny gripping force could not be transferred to slave end-

effector, EndoWrist [42], there are no problem to apply TTS to EndoWrist's movement modeling. Using the posture angles as the input and the gripping forces as the output, a model of the EndoWrist's inner mechanism is developed. Next, the values of expected gripping force obtained from the model are compared with actual measurements from da Vinci EndoWrist to verify and validate the model. The specific contents of EIMM are described in section 2.1.

1.3.2. Novel End-effector and Mater Interface

The da Vinci surgical robot system's EndoWrist is reported to have different gripping forces for different wrist postures [21]. This limitation is considered to arise from the joints of the gripping motion, which is used for generating driving force, being coupled with other joints through mechanical strings. This problem similarly arises in aerospace engineering, where a pilot's control stick is connected to the wing's control surfaces through mechanical strings, cables, or many mechanical parts [43-45]. In this field, most of these problems are resolved by adopting a Fly-By-Wire (FBW) system that directly drives the wing control parts, such as the control surfaces, using the ends of the wing's actuators and eliminates the need for mechanical strings [46, 47]. In the airplane with the FBW system, almost all mechanical connection parts for wing control are replaced with electrical wire for reliable control [48]. This aerospace

technology has inspired a novel concept; Surgical-Operation-by-Wire (SOBW) [49, 50].

In the medical field, the present research aims to develop a SOBW concept. The SOBW, which is first defined in this research, is a concept which replaces mechanical strings with electrical wire in the surgical robot system. Similar concept of SOBW is revealed in the existing surgical robot system; da Vinci robot which could be regarded as a semi-SOBW system because it uses many mechanical strings in internal parts. In the proposed surgical robot system, all mechanical strings are therefore removed and all joints are driven directly by actuators such as Alternative Current (AC) servo motors in the external arm and micro motors in surgical instrument with a diameter of 8 mm for full SOBW system (KS-4). However, previous studies have shown that motions such as pitching, yawing, rolling, and gripping cannot be integrated into an 8 mm diameter [28, 51-53]. Furthermore, while a micro motor is appropriate for moving the joint, it cannot provide sufficient gripping force. So, it is necessary to develop a new gripping system. A new type of pneumatic end-effector is developed for the gripping motion. The gripping force is adjustable by the controlling pressure using a pneumatic system consisting of a compressor, air pump, 3-way Solenoid Valves (SVs), speed controller, pressure controller, and catheter balloon which tolerates high pressure for clinical use [54]. This gripping system is decoupled from the external arm and the pitching/yawing joint, unlike existing laparoscopic surgical robots. Therefore, sufficient gripping force is obtained and maintained regardless of the end-effector's

different postures. Through repeated gripping experiments, the surgical instrument's durability is verified. In this research, the surgical robot system adopts a Hands-On-Throttle-And-Stick (HOTAS) controller for the surgeon's control interface. HOTAS is used for flight control in the aerospace field, and it can control hundreds of functions and provide feedback to the pilot about flight conditions. Similarly, it can be used to help surgeons perform many surgical operations, and it can be easily applied to force feedback research. The 6-axis robot is integrated with the proposed surgical instrument for a surgical peg task with the aim of examining the clinical applicability of the proposed system. This novel surgical robot system can be widely used for laparoscopic robotic surgery.

2. Materials and Methods

2.1. EndoWrist Inner Mechanism Model

To quantitatively model EndoWrist's inner mechanism, the formulas shown in equations (2.1), (2.2), and (2.3) were proposed in this research.

$$F = C \cdot f(\alpha, \beta, \gamma) \tag{2.1}$$

$$F = C_0 + C_\alpha \cdot \alpha + C_\beta \cdot \beta + C_\gamma \cdot \gamma + C.T. + H.D.P.$$

$$\cong \begin{bmatrix} C_0 & C_\alpha & C_\beta & C_\gamma \end{bmatrix} \begin{bmatrix} 1 & \alpha & \beta & \gamma \end{bmatrix}^T \tag{2.2}$$

$$\begin{pmatrix} F_{M_1} \\ F_{M_2} \\ F_{M_3} \\ F_{M_4} \end{pmatrix} = \begin{pmatrix} 1 & \alpha_1 & \beta_1 & \gamma_1 \\ 1 & \alpha_2 & \beta_2 & \gamma_2 \\ 1 & \alpha_3 & \beta_3 & \gamma_3 \\ 1 & \alpha_4 & \beta_4 & \gamma_4 \end{pmatrix} \begin{pmatrix} C_0 \\ C_\alpha \\ C_\beta \\ C_\gamma \end{pmatrix} \tag{2.3}$$

The real gripping force (F) is shown in equation (2.1) where C and $f(\alpha,\beta,\gamma)$ are unknown coefficients and unknown function of Euler angles, respectively. Next, equation (2.1) was re-written as a summation of linear model term, Coupled-Terms (C.T.), and Higher-Degree-Polynomials (H.D.P.); then, it was simplified with linear model terms, as shown in equation (2.2). In this research, a simplified, linear model was investigated and the C.T. and/or H.D.P. will be added if the linear model is inadequate.

A gripping force for the 27 Euler angle combinations was measured, and then, 4 out of the 27 measured gripping forces ($F_{M_1}, F_{M_2}, F_{M_3}, F_{M_4}$) were used to compute the four unknown coefficients ($C_0, C_\alpha, C_\beta, C_\gamma$) shown in equation (2.3). The 23 remaining measured gripping forces were used for validation. In this way, ${}_{27}C_4$, which is 17,750 sets of coefficients, are obtained, and 17,750 sets were analyzed. For estimating each EndoWrist's unknown coefficients additionally, the least square method that was a standard approach to the approximate solution of overestimated system was also used. The overdetermined parameters, 27 Euler angle posture and measured gripping force results, were applied to equation (2.4).

$$F = AC, \quad \textit{(A: Euler angle sets \& C: Coefficient sets)}$$

$$\begin{pmatrix} F_{M_1} \\ \vdots \\ F_{M_{27}} \end{pmatrix} = \begin{pmatrix} 1 & \alpha_1 & \beta_1 & \gamma_1 \\ \vdots & \vdots & \vdots & \vdots \\ 1 & \alpha_{27} & \beta_{27} & \gamma_{27} \end{pmatrix} \begin{pmatrix} C_0 \\ C_\alpha \\ C_\beta \\ C_\gamma \end{pmatrix} \tag{2.4}$$

Because Euler angle set matrix is not invertible, equation (2.4) is solved as shown in equation (2.5).

$$C = (A^T A)^{-1} A^T F \tag{2.5}$$

The obtained coefficients are substituted into equation (2.4) and error is analyzed for all experimental results.

2.2. Development of the Laparoscopic Robot

A control flow of the entire system is depicted in Fig. 2.1. The system consists of the HOTAS interface that can reflect the surgeon's decision, the control 6-axis external robot arm, and the surgical instrument with the pneumatic control system. To improve the function of the HOTAS controller, a 6-axis force/torque sensor (Dynpick, Wacoh-Tech Inc., Takaoka City, Futatsuka, Japan) was attached to the bottom in a special housing as shown in Fig. 2.2. A threaded upper and lower assembly parts of 6-axis force/torque sensor were attached with special housing's upper and lower layer, respectively. All the screws in the special housing assembly were tightly secured to ensure the precise measurement. The improved HOTAS (iHOTAS) controller was used to perform translational movement [55-57]. Hardware related to the surgical robot system were integrated with LabVIEW® and PXIe controller (LabVIEW® 2013, PXIe-8135 & 1062Q, NI, Used valid license). Air flow control of the pneumatic system using two SVs was executed by a data acquisition board (USB-6212 DAQ, NI). The pitching/yawing joints of the surgical instrument were controlled by a micro motor and a motor controller (EC-4 motor, EPOS2 controller, Maxon Motor, Brünigstrasse, Sachseln, Switzerland).

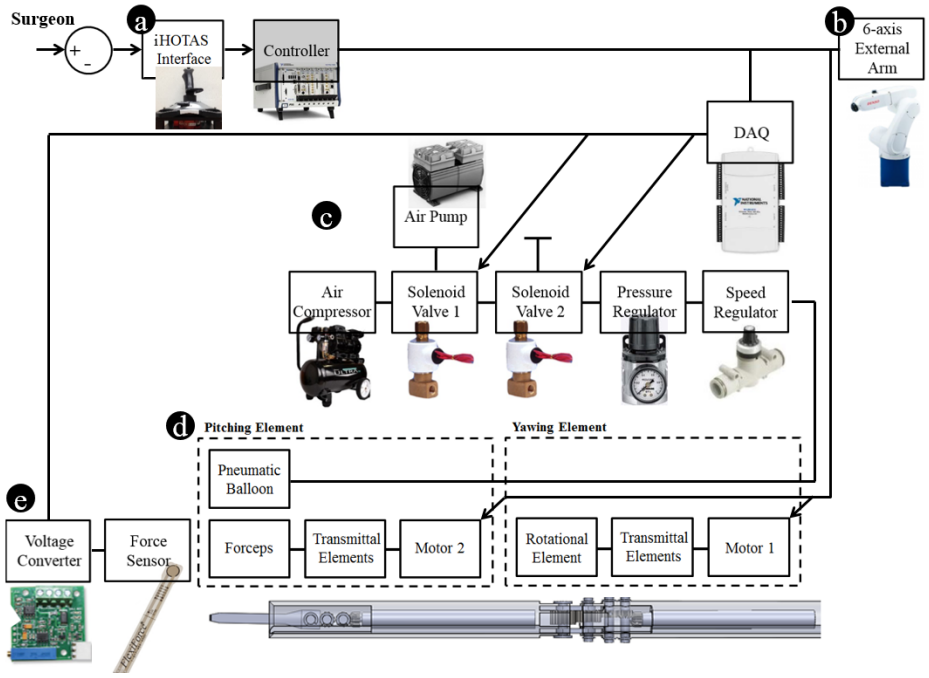

Fig. 2.1 Control block diagram and experimental flow of the overall system.

(a) Interface for surgeon. (b) External arm. (c) Pneumatic gripper system. (d) Surgical instrument (KS-4). (e) Gripping force measurement system using data acquisition (DAQ) board. All hardware is controlled using the LabVIEW® software based on the state machine structure.

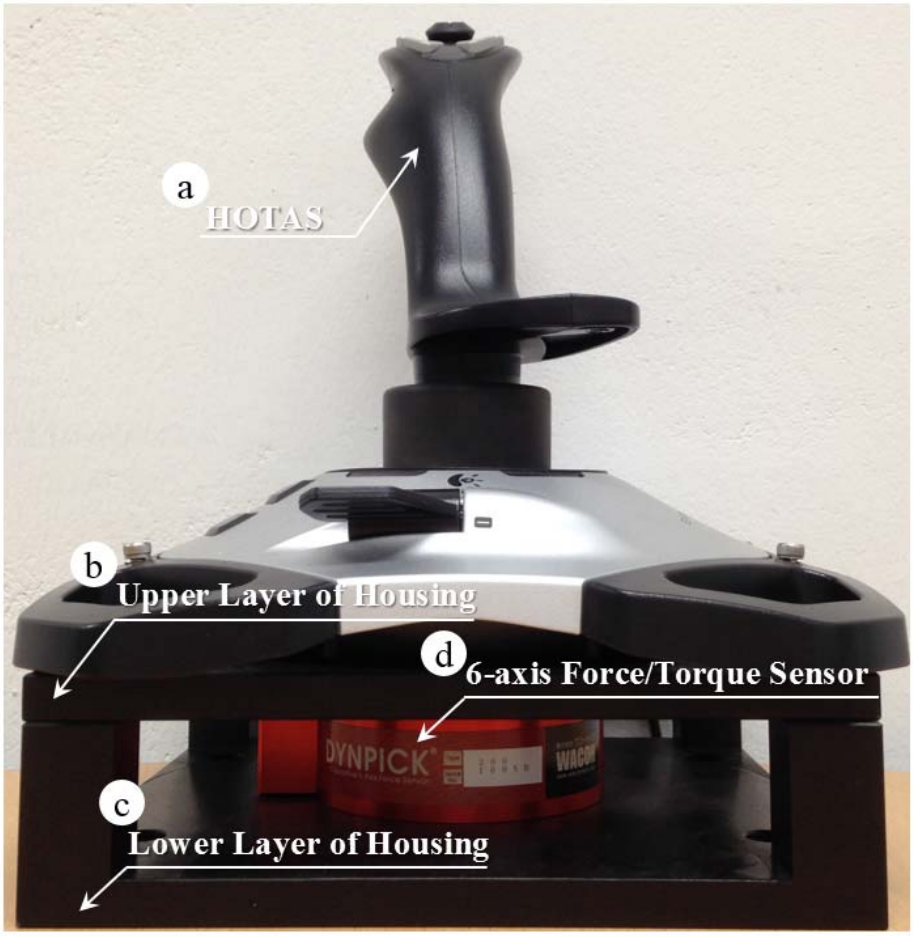

Fig. 2.2 Improved Hands-On-Throttle-And-Stick (iHOTAS).

(a) Conventional HOTAS controller. (b) Upper layer of the special housing**.** (c) Lower layer of the special housing. (d) 6-axis force/torque sensor. All the screws in the special housing assembly were tightly secured to ensure the precise measurement. The improved HOTAS (iHOTAS) controller was used to perform translational movement.

2.2.1. Overview

The proposed surgical robot system could be divided into two parts: external arm and surgical instrument (KS-4). The former could perform 6-DOF movements including translational motion, fulcrum point motion, and the surgical instrument's rolling motion. The latter could perform 2-DOF movements such as the yawing and pitching motions and gripping motion. A pneumatic gripper was installed at the end of the surgical instrument. Because the external arm and the surgical instrument were decoupled, unlike in almost all other surgical robot systems [5, 26, 58], the surgical instrument could be detached from the external arm and be easily replaced during surgery. The executing force of the surgical robot system was generated by six AC servo motors (VS-6556G, DENSO, Kariya, Aichi Prefecture, Japan), two micro motors (EC-4 & 280:1 ∅4 planetary gearhead, Maxon Motor), and a pneumatic compressor (ULTRA 224, AirFactory, Seoul, South Korea).

2.2.2. External Arm

For translational motion, fulcrum point motion, and the surgical instrument's rolling motion, a 6-axis external arm (VS-6556G, DENSO) was utilized. In Fig.

2.3, *J1-J5* are complexly involved with the translational motion and fulcrum point motion. *J6* independently executes the surgical instrument's rolling motion. The complex movements of *J1-J5* were controlled by tool coordinates. The tool coordinates set the external arm's origin to the origin of the end-effector. The external arm moves on the basis of the fulcrum point and translational motion according to the user's iHOTAS control.

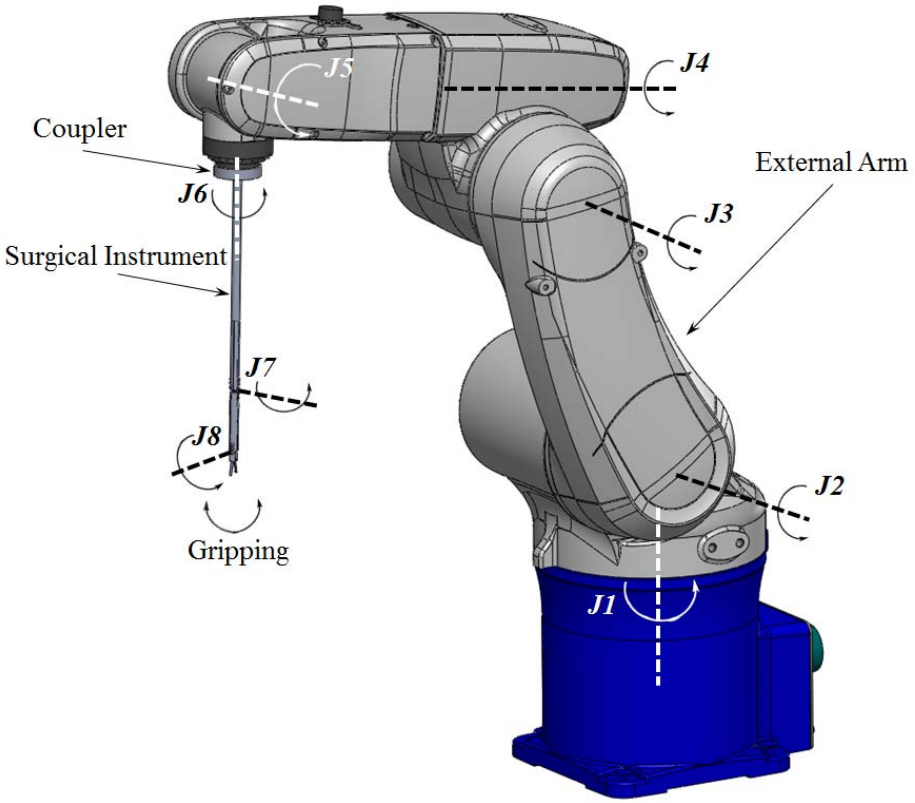

Fig. 2.3 Conceptual design of the surgical robot system.

2.2.3. End-effector (KS-4)

The flexion/extension motions of the wrist were performed using the surgical instrument's pitching motion in *J8*. The radial/ulnar deviation motions of the wrist could be overcome by a combination of the surgical instrument's pitching motion (*J8*) and rolling motion (*J6*, external arm). The flexion and supination motions of the elbow could be compensated by the surgical instrument's yawing motion (*J7*) and rolling motion (*J6*, external arm), as shown in Fig. 2.3. The ranges of elbow and wrist joint were 36° and 60°, respectively. An elbow joint would be helpful in decreasing the probability of the surgical instruments' collision with the outside of the abdominal cavity [26]. The driving force of the surgical instrument's pitching and yawing motion was not generated using mechanical strings, as in other systems [26, 58, 59]. Micro motors were used to perform pitching and yawing motions in the outer shells, as shown in Figs. 2.4 and 2.5. The surgical instrument which removed coupler and extension part from Figs. 2.4 and 2.6 was shown in Fig. 2.5. This figure represented the actual gripper, elbow joint, and wrist joint in detail. The gripper could be closed by inflating catheter balloons as shown in Fig. 2.5-(c). Outer shells were manufactured using a 3-D printer (Form 1, Formlabs, Somerville, MA, USA) to the nearest sub-millimeter resolution and to assemble several parts such as micro motors, gears, and joint links. The surgical instrument was 300 mm long for surgical usability. The outer diameter was 8 mm, the same as that of the da

Vinci surgical robot system's EndoWrist, for MIS. In addition, the driving force of gripping motion was generated from the pneumatic system's compressor.

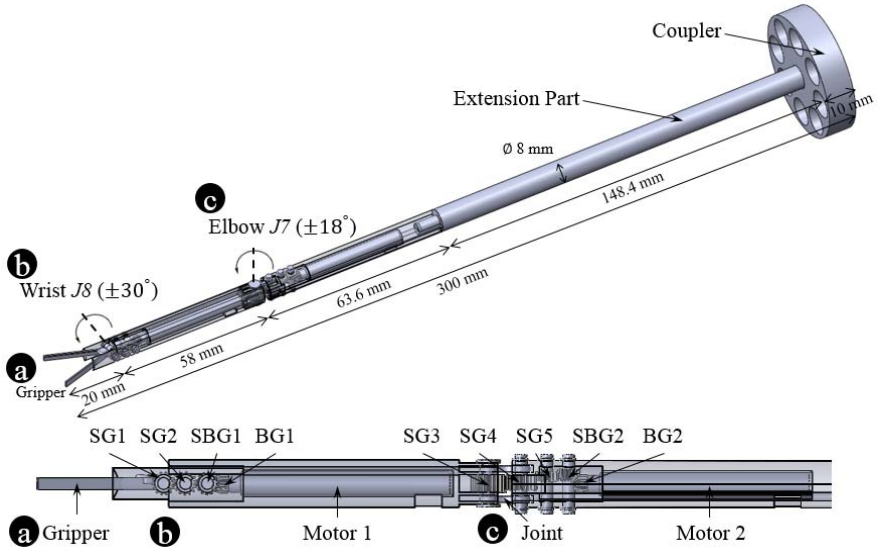

Fig. 2.4 Design of surgical instrument (KS-4). (a) Pneumatic gripper**.** (b) Wrist joint. (c) Elbow joint. Several gears, outer shells, micro motors, and joint link are assembled. This instrument performs elbow, wrist, and gripping motions. The surgical instrument's length and outer diameter are 300 mm and 8 mm, respectively.

* Abbreviation: Spur Gear (SG), Spur and Bevel Gear (SBG), and Bevel Gear (BG).

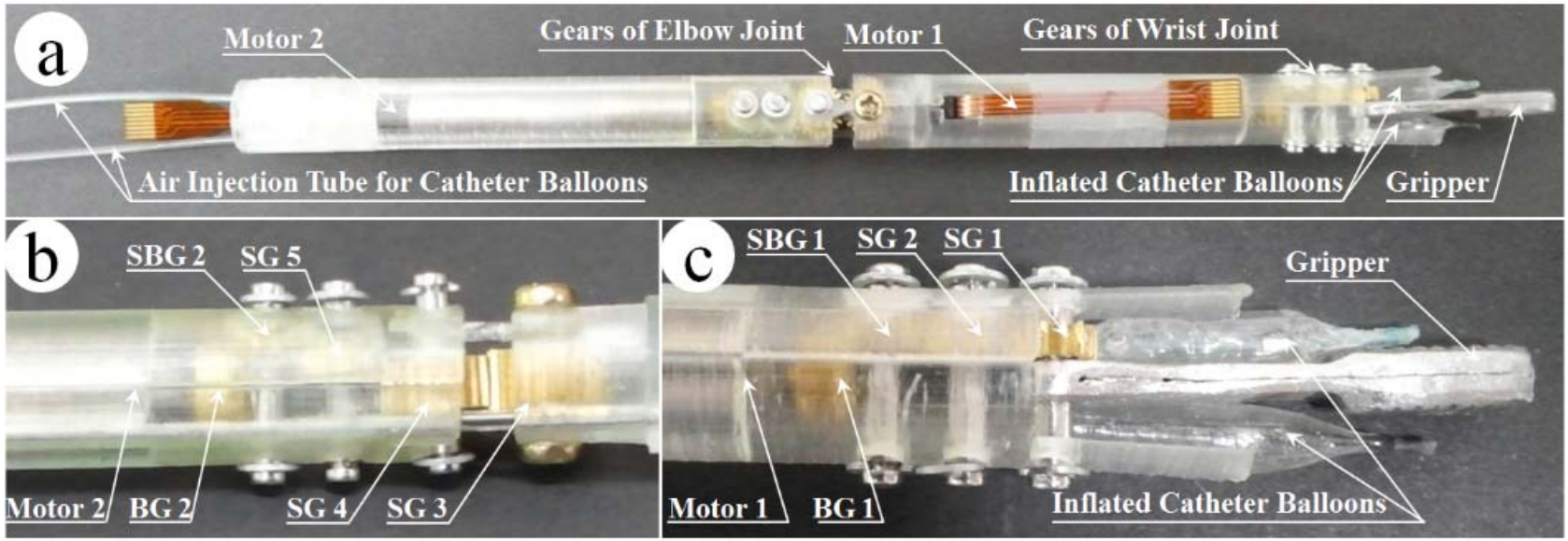

Fig. 2.5 Actual surgical instrument (KS-4). (a) Entire surgical instrument. (b**)** Zoom in for elbow joint. (c) Zoom in for wrist joint and closed gripper by inflated catheter balloons. The position of the micro motors, several gears, and gripper are presented in this figure. The inflated catheter balloons make gripper close the gripper's tips by Newton's 3rd law.

The pneumatic gripping system enabled complex yawing and pitching movements, provided sufficient gripping force, and was decoupled from the external arm within an 8 mm outer diameter. The pitching motion could be directly actuated by the micro motor if the micro motor was able to tolerate weight of the gripper and the yawing motion could be achieved when the micro motor could tolerate the weight of elbow part, which was consist of the gripper, one micro motor, five gears, and outer shell. The weight of the whole surgical instrument was 36 g. The weights of the driving parts (elbow and wrist part) of surgical instrument and extension part with coupler were 15 g and 21 g, respectively. As for the elbow part in driving parts, it only occupied 7 g. Since the micro motor had the torque of 0.0473 N·m (0.4827 kgf·cm = 482.7gf·cm, the efficiency of the micro motor and planetary gearhead were considered) by using 280:1 of gear rate, it was sufficiently able to tolerate the weight as mentioned above.

Fig. 2.6 Assembled surgical instrument (KS-4) and external arm.

2.2.3.1. Pneumatic Gripper System

The gripping motion was achieved by inflating and deflating the catheter balloon. The air compressor and air pump were used to pump compressed air into and suck the same out of the catheter balloon, respectively. The compressed air was controlled using SVs, a speed regulator, and a pressure regulator, as shown in Fig. 2.7. The surgeon's decision was reflected by the pneumatic gripper system, as shown in Fig. 2.8. To control the gripping motion, two SVs were controlled with one of three statuses: inflow, stay, and outflow. In Fig. 2.9, compressed air flowed from the compressor to the surgical instrument's catheter balloon via SV1 and SV2 for the inflow status (SV1 and SV2: On). It could inflate the catheter balloon to close the gripper. Compressed air could not be flowed into the surgical instrument and halted at SV2 for the stay status (SV1: On, SV2: Off). For opening the gripper in the outflow status, SV1 and SV2 were turned off and on, respectively. At this time, the remaining compressed air in the surgical instrument flowed to the atmosphere by the air pump.

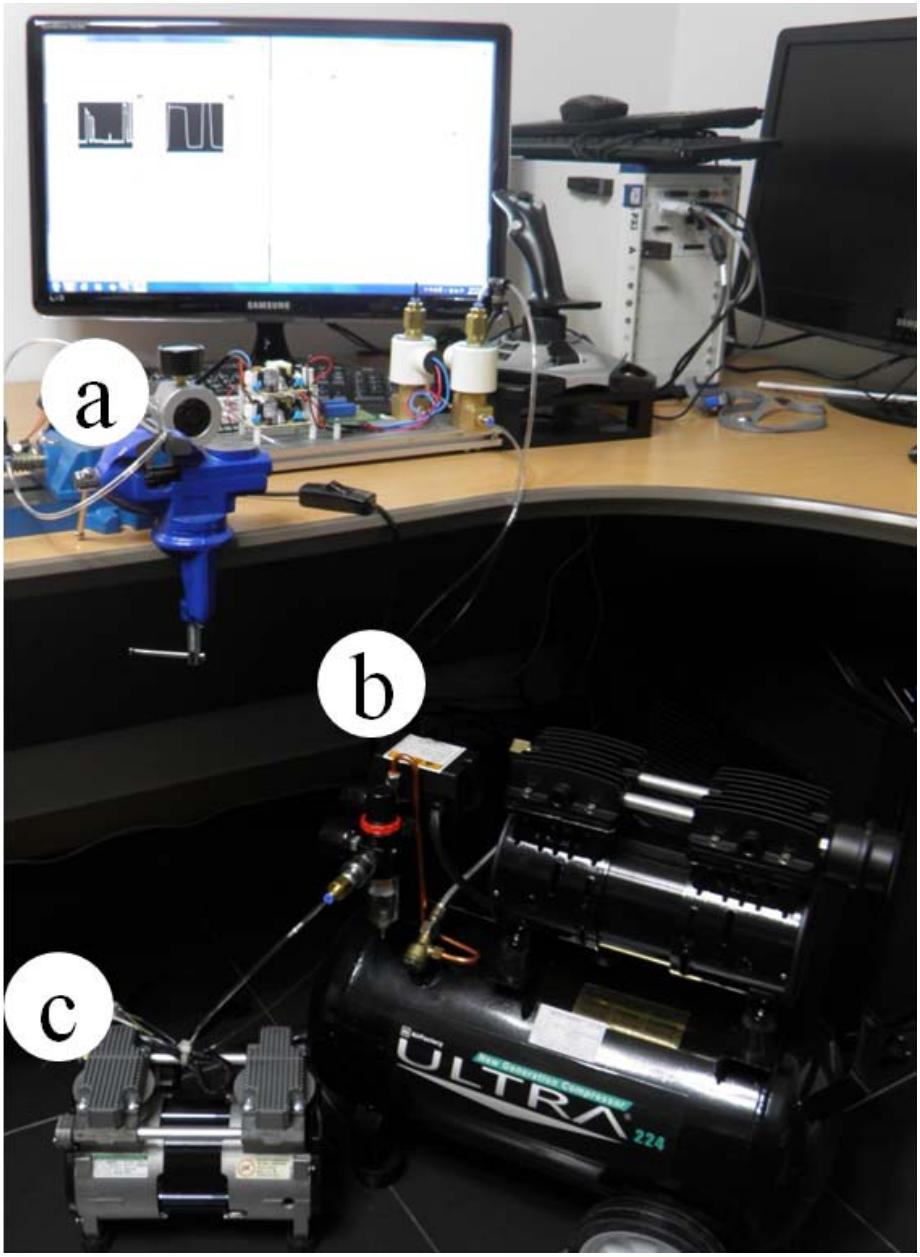

Fig. 2.7 Pneumatic hardware system. (a) Solenoid valves, speed regulator, and pressure regulator control the compressed air. (b) Air compressor pumps compressed air into the catheter balloon. (c) Air pump sucks compressed air out of the catheter balloon.

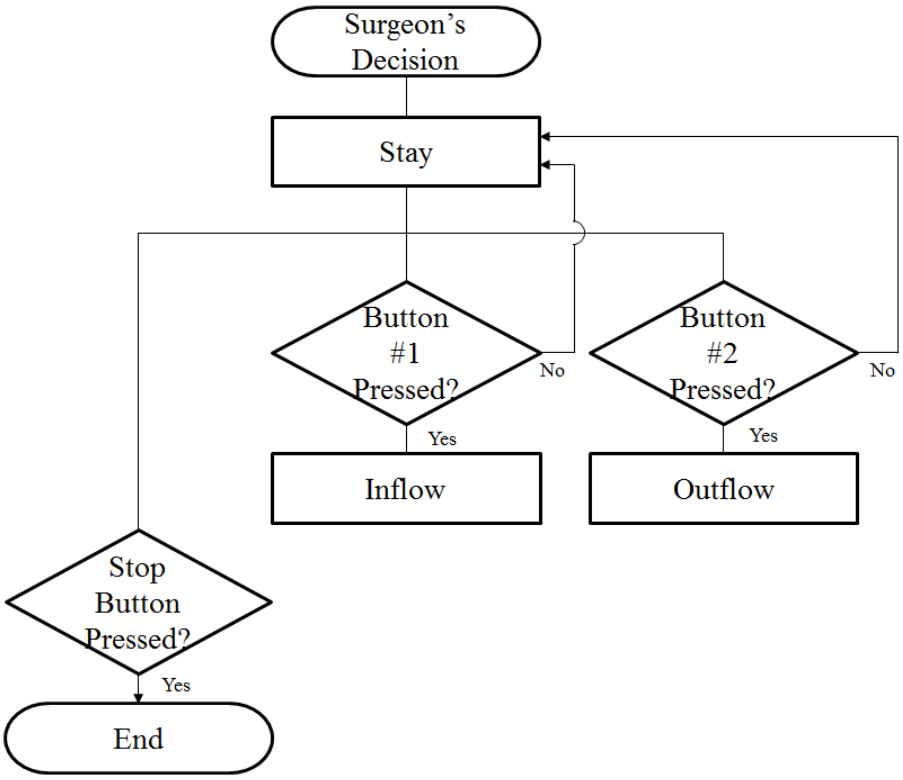

Fig. 2.8 Diagram of valve control algorithm. Three valve statuses can be controlled by the surgeon.

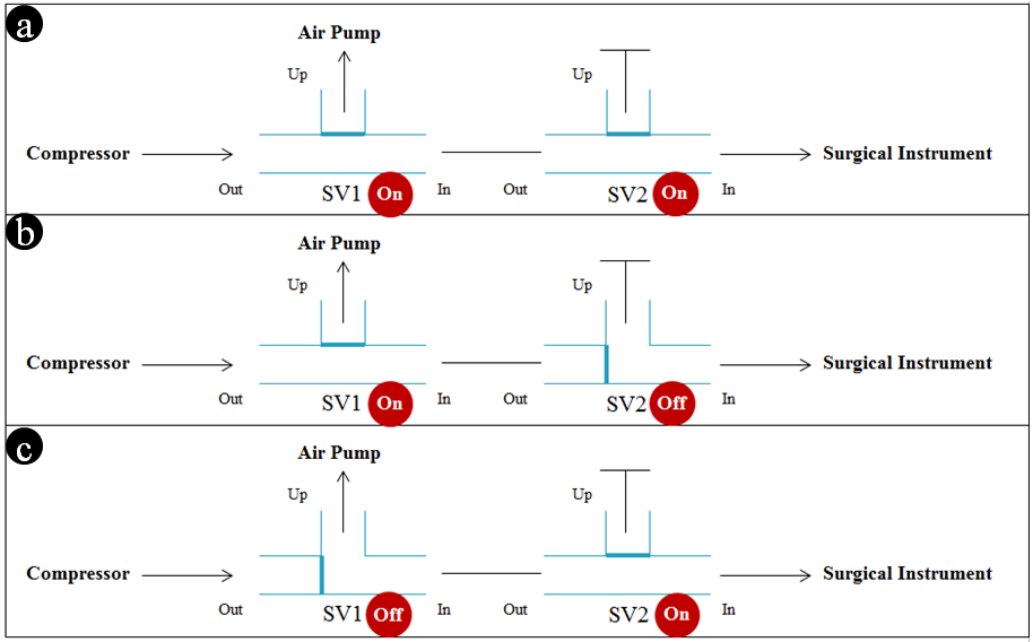

Fig. 2.9 Compressed air flow by valve mechanism. (a) Inflow. (b) Stay. (c) Outflow. Three compressed air flow statuses are controlled by SV1 and SV2 between the compressor and the catheter balloons.

* Abbreviation: Solenoid Valve (SV).

Table 2.1 The mapping between iHOTAS and surgical robot system

iHOTAS	External Arm	End-effector (KS-4)
Stick's x-axis direction Dynpick's x-axis force Dynpick's z-axis torque	x-axis fulcrum motion	
Stick's y-axis direction Dynpick's y-axis force Dynpick's z-axis torque	y-axis fulcrum motion	
Dynpick's z-axis force	Translational motion	
Dynpick's z-axis torque	Rolling motion (*J6*)	
Button #1		Gripper (Close)
Button #2		Gripper (Open)
POV-left/right		Wrist motion (*J8*)
POV-up/down		Elbow motion (*J7*)
Throttle	Adjust the scale of motion	

The translational motion and fulcrum point motion was complexly involved with J1-J5. A Dynpick's voltage output signal was calibrated and filtered as described in section 1.3.1.. The fulcrum motions of x & y-axis were achieved by collecting several signals (stick's directions, Dynpick's force/torque) which reflects surgeon's decision entirely.

* Abbreviation: improved Hands-On-Throttle-And-Stick (iHOTAS) and Point Of View (POV).

2.2.4. Forward Kinematics of the System

Fig. 2.10 shows the kinematic structure of the entire system, except for the gripping motion. *J1-J6* and *J7-J8* represent the external arm parts and surgical instrument (KS-4), respectively. Table 2.2 shows the Denavit-Hartenberg (D-H) parameters of this system.

Table 2.2 Forward kinematics of the system (D-H parameters)

Joint	α_{i-1}	a_{i-1}	d_i	θ_i
1	0	0	335	θ_1
2	$-\frac{\pi}{2}$	75	0	$\theta_2 - \frac{\pi}{2}$
3	0	270	0	θ_3
4	$-\frac{\pi}{2}$	90	295	θ_4
5	$\frac{\pi}{2}$	0	0	θ_5
6	$-\frac{\pi}{2}$	0	296	$\theta_6 + \frac{\pi}{2}$
7	$\frac{\pi}{2}$	0	0	$\theta_7 + \pi$
8	$-\frac{\pi}{2}$	58	0	θ_8

Forward kinematics and Denavit-Hartenberg (D-H) parameters of the overall system are defined by Fig. 2.10 and Table 2.2. The external arm and surgical instrument are executed using several control algorithms.

With reference to Table 2.2, each joint's information such as operational angle and other information could be confirmed. These homogeneous transformation matrices are inferred from D-H convention theory [60]. From these parameters, equation (2.6) [60], and Fig. 2.10, the homogeneous transformation matrices of the proposed system's each joint could be obtained. According to equation (2.6), each joint is designated to unique homogeneous transformation matrix.

$$ {}^{i-1}_{i}T = \begin{bmatrix} cos(\theta_i) & -sin(\theta_i) & 0 & a_{i-1} \\ \sin(\theta_i)cos(\alpha_{i-1}) & \cos(\theta_i)\cos(\alpha_{i-1}) & -sin(\alpha_{i-1}) & -\sin(\alpha_{i-1})d_i \\ sin(\theta_i)\sin(\alpha_{i-1}) & cos(\theta_i)\sin(\alpha_{i-1}) & cos(\alpha_{i-1}) & cos(\alpha_{i-1})d_1 \\ 0 & 0 & 0 & 1 \end{bmatrix} \tag{2.6} $$

Each joint's information such as operational angle and other information could be confirmed. From these parameters, the homogeneous transformation matrices are given as (12)–(19).

$$ {}^{0}_{1}T = \begin{bmatrix} cos\theta_1 & -sin\theta_1 & 0 & 0 \\ sin\theta_1 & cos\theta_1 & 0 & 0 \\ 0 & 0 & 1 & d_1 \\ 0 & 0 & 0 & 1 \end{bmatrix} \tag{2.7} $$

$$ {}^{1}_{2}T = \begin{bmatrix} sin\theta_2 & cos\theta_2 & 0 & a_1 \\ -cos\theta_2 & sin\theta_2 & 0 & 0 \\ 0 & 0 & 1 & 0 \\ 0 & 0 & 0 & 1 \end{bmatrix} \tag{2.8} $$

$$ {}^{2}_{3}T = \begin{bmatrix} cos\theta_3 & -sin\theta_3 & 0 & a_2 \\ sin\theta_3 & cos\theta_3 & 0 & 0 \\ 0 & 0 & 1 & 0 \\ 0 & 0 & 0 & 1 \end{bmatrix} \tag{2.9} $$

$$ {}^{3}_{4}T = \begin{bmatrix} cos\theta_4 & -sin\theta_4 & 0 & a_3 \\ 0 & 0 & 1 & d_4 \\ -sin\theta_4 & -cos\theta_4 & 0 & 0 \\ 0 & 0 & 0 & 1 \end{bmatrix} \tag{2.10} $$

$$ {}^{4}_{5}T = \begin{bmatrix} cos\theta_5 & -sin\theta_5 & 0 & 0 \\ 0 & 0 & -1 & 0 \\ sin\theta_5 & cos\theta_5 & 0 & 0 \\ 0 & 0 & 0 & 1 \end{bmatrix} \tag{2.11} $$

$$ {}^{5}_{6}T = \begin{bmatrix} -sin\theta_6 & -cos\theta_6 & 0 & 0 \\ 0 & 0 & 1 & d_6 \\ -cos\theta_6 & sin\theta_6 & 0 & 0 \\ 0 & 0 & 0 & 1 \end{bmatrix} \tag{2.12} $$

$$ {}^{6}_{7}T = \begin{bmatrix} -cos\theta_7 & sin\theta_7 & 0 & 0 \\ 0 & 0 & -1 & 0 \\ -sin\theta_7 & -cos\theta_7 & 0 & 0 \\ 0 & 0 & 0 & 1 \end{bmatrix} \tag{2.13} $$

$$ {}^{7}_{8}T = \begin{bmatrix} cos\theta_8 & -sin\theta_8 & 0 & a_7 \\ 0 & 0 & 1 & 0 \\ -sin\theta_8 & -cos\theta_8 & 0 & 0 \\ 0 & 0 & 0 & 1 \end{bmatrix} \tag{2.14} $$

The transformation matrices of the external arm and surgical instrument are given by (2.15) and (2.16), respectively. Equation (2.15) describes the position and orientation of the external arm's translational and fulcrum point movements and equation (2.16), the surgical instrument's position and orientation. This corresponded to the surgical robot's pitching and yawing motions. The

transformation matrix of the overall system is given by (2.17).

$$ {}^{0}_{6}T = {}^{0}_{1}T\,{}^{1}_{2}T\,{}^{2}_{3}T\,{}^{3}_{4}T\,{}^{4}_{5}T\,{}^{5}_{6}T \tag{2.15} $$

$$ {}^{6}_{8}T = {}^{6}_{7}T\,{}^{7}_{8}T \tag{2.16} $$

$$ {}^{0}_{8}T = {}^{0}_{1}T\,{}^{1}_{2}T\,{}^{2}_{3}T\,{}^{3}_{4}T\,{}^{4}_{5}T\,{}^{5}_{6}T\,{}^{6}_{7}T\,{}^{7}_{8}T \tag{2.17} $$

The transformation matrix of the external arm is calculated as a series of multiplication of the *J1*-*J6*'s homogeneous transformation matrices. The transformation matrix of the surgical instrument is calculated in a similar way (using *J7*-*J8*'s homogeneous transformation matrices). The above two transformation matrices describe; i) the position & orientation of the external arm's translational & fulcrum point movements and ii) the surgical instrument's position & orientation, respectively. The transformation matrix of the overall system is calculated from the multiplication of the above two transformation matrices [60].

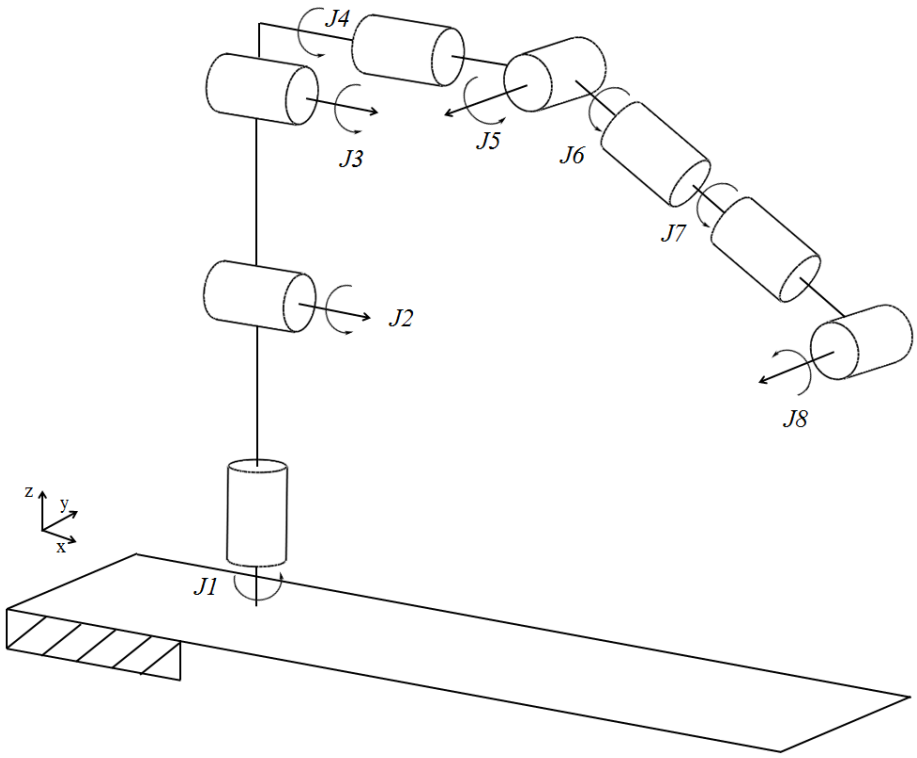

Fig. 2.10 Kinematic structure of the system.

3. Results

3.1. Prediction of the Compensation Force for EndoWrists

3.1.1. EndoWrist's Gripping Force

For the 27 cases for each EndoWrist, the gripping forces were measured 5 times, and the Mean Gripping Force (MGF) and the Standard Deviation (SD) were computed (Table 1.3). The overall MGF and the overall SD for the P.F. EndoWrist were 15.30 N and 0.35 N, respectively. The overall mean (and SD) of P.D.F. and L.N.D. EndoWrist were measured in 7.87 N (0.13 N) and 11.65 N (0.27 N), respectively. The ratio of the SD to the MGF had a minimum of 1.65% (in P.D.F.) and a maximum of 2.32% (in L.N.D.). As a result, the experimental set-up and the measurement process were acceptable for test. However, it was observed that the MGF for the 27 cases were significantly different. The P.F. EndoWrist was measured at 20.33 N in A(0˚, 0˚, -90˚) and

11.05 N in A(0˚, 70˚, -90˚). The L.N.D. was measured at 17.73 N in A(90˚, 70˚, -90˚) and 6.81 N in A(0˚, 70˚, 0˚). Especially for the P.D.F. EndoWrist, the MGF for two different postures A(90˚, 70˚, -90˚) and A(-90˚, 70˚, 90˚) were 14.15 N and 4.20 N, respectively. These results imply that the EndoWrist exerts a different gripping force for a minimum of 1.84 times more (in P.F.) and a maximum of 3.37 times more (in P.D.F.) in each posture, even if the surgeon exerts the same amount of force. The maximum and minimum values of MGF were observed most frequently at the yaw angles of 90˚ and -90˚.

The L.N.D.'s measured gripping force results among the three EndoWrists used in this research were directly comparable with the reference's results using the actual da Vinci [21]. They conducted the research for the five postures (Neutral, Minor Deflection Right, Minor Deflection Left, Major Deflection Up, and Major Deflection Down) and they were corresponded with Euler angle sets ((0˚, 0˚, 0˚), (0˚, 0˚, 90˚), (0˚, 0˚, -90˚), (0˚, 70˚, 0˚) and (0˚, -70˚, 0˚)), which was proposed in this research, respectively. The gripping forces for the posture of (0˚, 0˚, 90˚)/'Minor Deflection Right' were slightly bigger than that of the posture of (0˚, 0˚, 0˚)/'Neutral'. These values were slightly smaller than the gripping force for the posture of (0˚, 0˚, -90˚)/'Minor Deflection Left'. These three postures' gripping forces had similar results. The gripping forces for the posture of (0˚, 70˚, 0˚)/'Major Deflection Up' had the smallest value in both experiments with a sharp decrease. The gripping forces for the posture of (0˚, -70˚, 0˚)/'Major Deflection down' were slightly bigger than that of the posture of (0˚, 70˚, 0˚)/'Major Deflection Up'. In other words, the tendencies about five

postures were exactly same for the results in this research and actual da Vinci system's results. From these comparisons, up/down motions of the EndoWrist had a greater effect on gripping force than right/left motions.

3.1.2. Prediction Results and Validation

From the Table 1.3, four randomly chosen measured gripping forces were selected to compute the four unknown coefficients shown in linear model equation (2.3) because at least four results of the measured gripping force ($F_{M_1}, F_{M_2}, F_{M_3}, F_{M_4}$) and four different posture information (A($\alpha_i, \beta_j, \gamma_k$) for four different sets of (*i, j, k*)) were required to solve linear model equation (2.3). A set of coefficients: $C_0, C_\alpha, C_\beta,$ and C_γ was calculated by selecting four results among the 27 results. The remaining 23 gripping forces were used to validate the coefficient's error. This process was repeated with all of the 17,750 sets ($_{27}C_4$=17,750) of coefficients, and the optimal sets for three different EndoWrists with errors are summarized in Table 3.1. The four different Euler angles for three different EndoWrists shown in Table 3.1 were used in calculating optimal coefficient among 27 postures in accordance with measured mean gripping force in Table 1.3. C_0 means that the offset of EndoWrist is oriented by a mechanical characteristic of EndoWrist. Coefficients: $C_0, C_\alpha, C_\beta,$ and C_γ correspond to the roll, pitch, and yaw of the joint

characteristics. For the P.D.F. and L.N.D. EndoWrist, a set of coefficients with errors of 16.25% and 13.03% were obtained. Specifically, in the case of P.F., the lowest error was calculated as 10.69% where the lowest error means that P.F. EndoWrist is most predictable and less sensitive for the EndoWrist's posture changes.

The errors of least square method were higher than the prediction errors of linear model (Equ. (2.3)) as shown in Table 3.2.

Table 3.1 Optimal coefficient sets of EndoWrists and validation errors using linear model

EndoWrist	Angle (Degree, ˚)			Coefficients				Error (%)
	Roll (α)	Pitch (β)	Yaw (γ)	C_0	C_α	C_β	C_γ	
P.F.	-90	70	0	15.62	-0.71	-0.65	0.14	10.69
	0	0	-90					
	90	70	-90					
	90	70	90					
P.D.F.	-90	0	0	7.76	1.6	0.42	-0.31	13.03
	-90	70	90					
	90	-70	90					
	90	70	0					
L.N.D.	-90	-70	-90	12.23	0.74	-0.54	0.89	16.25
	-90	70	-90					
	-90	70	90					
	90	0	-90					

* Abbreviation: Prograsp Forceps (P.F.), PK Dissecting Forceps (P.D.F.), and Large Needle Driver (L.N.D.).

Table 3.2 Estimated coefficient sets of EndoWrists and validation errors using least square method

EndoWrist	Coefficients				Error (%)
	C_0	C_α	C_β	C_γ	
P.F.	16.61	-0.37	-0.15	0.05	11.00
P.D.F.	8.35	1.81	0.45	0.41	16.54
L.N.D.	13.59	0.17	0.16	0.59	17.45

* Abbreviation: Prograsp Forceps (P.F.), PK Dissecting Forceps (P.D.F.), and Large Needle Driver (L.N.D.).

3.2. Pneumatic Type of End-effector (KS-4) and Novel Master Interfaces

3.2.1. End-effector's Gripping Force

3.2.1.1. Gripping Force System Setup

The gripping force was measured using a flexible piezo-resistive sensor (Flexiforce, Tekscan Inc.) as shown in Fig. 3.1. Flexiforce is widely used for pressure measurement in medical applications, and its linearity has been demonstrated [61]. The gripper can be closed by the force generated by Newton's 3rd law as the inflated catheter balloon pushes the outer shell. To estimate the relationship equation (3.1) between Flexiforce's output value and force value, six precision weights (50 g, 100 g, 200 g, 500 g, 1 kg, and 2 kg) were placed on the Flexiforce in order and the output voltages values were measured and converted into force values through a specific LabVIEW® algorithms.

$$F_{orce} = (1{,}172.4 \times V_{oltage} - 14.5) \times 9.81 \qquad (3.1)$$

Fig. 3.1 Gripping force measurement experimental setup using Flexiforce.

The output voltages of Flexiforce were recorded using a data acquisition board (USB-6212 DAQ, NI). The initial data of 500 samples were used for sensor calibration and initialization in each experiment. For filtering spiky noise,

Savitzky-Golay filtering was applied to the signal processing [62, 63]. Signal processing was performed after the gripping force measurement experiment using MATLAB software.

The gripper which was manufactured from the existing stainless forceps (AE-4520-1, KASCO, Sialkot, Pakistan) with the modification on the size and the hole for connecting the gripper to the surgical instrument. In general, medical forceps has the restoring force which has tendency to keep the gripper opened. With our compressor being used in this research, it varied in elastic deformation are and was extremely difficult for making the plastic deformation status for forceps. Actually, gripper's restoring force became smaller as the tips of gripper became larger (in this case, displacement became larger). As a result, the gripping force ('force by catheter balloons' minus 'restoring force of gripper') became larger because force by catheter balloon was constant, which meant that the force suggested in this research (displacement between tip is 0) was the smallest force that could be made in this system. In the experiment, assumed that the thickness of Flexiforce and tissue were both thin, the force would be also similar.

3.2.1.2. Relationship between Compressor's Pressure and Gripping Force

The gripping force was measured 10 times for 0 to 0.775 MPa (interval: 0.025 MPa), and the results are plotted in Fig. 3.2. The standard deviation of the 10 measurements for each pressure was calculated and plotted in Fig. 3.2 as the error bar. The mean of all gripping forces' standard deviation was computed as 0.1 N. In Fig. 3.2, the pressure section can be divided into two sections except for 0.05 MPa—section 1 (0.1 - 0.35 MPa) and section 2 (0.375 - 0.775 MPa) by linearity. Equations (3.2) and (3.3) were derived. In sections 1 and 2, the gripping forces from the surgical instrument's gripper (*GF1* and *GF2*) were determined by pressure values from the compressor according to (3.2) and (3.3), respectively.

$$GF_1 = c_1 \mathrm{P} + i_1 \tag{3.2}$$

$$GF_2 = c_2 \mathrm{P} + i_2 \tag{3.3}$$

The coefficients: c_1, i_1, c_2 and i_2 of equation (3.2) and (3.3) were calculated as 2.2000, −0.7979, 0.6785, and 4.6910, respectively. The means of the differences between the linear equations (3.2) and (3.3) and the experimental results in Fig. 3.2 were 0.0938 N (standard deviation: 0.0665 N) and 0.0927 N (standard deviation: 0.0607 N) for sections 1 and 2, respectively. These mean values were within the total mean's standard deviation. This means that the above two equations can be inferred as significant results. These values were referred to in the other experiments conducted in this research.

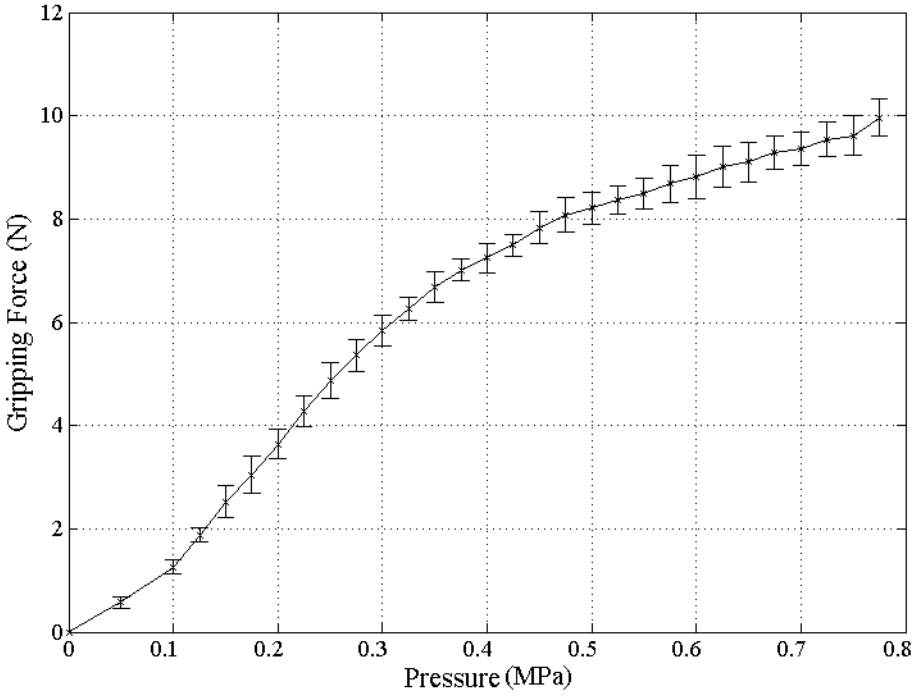

Fig. 3.2 Experimental result of gripping force in accordance with pressure during 10 repetitions. The standard deviation of the gripping force was 0.1 N between 0 and 0.775 MPa with 0.025 MPa intervals.

3.2.1.3. Reaction Time

The simulated results were determined by a step function using (24) at 0.3 MPa to be 5.8 N, as shown in Fig. 3.3. Because setting the pressure value as an experimental variable was meaningless for the purpose of the reaction time experiment, a 0.3 MPa was chosen as a representative value. The ideal step

function was co-plotted with the experimental results filtered by the Savitzky-Golay filter. This experiment was automatically conducted using a specific LabVIEW® algorithm for excluding users' irregular HOTAS triggers and repeating the same trigger time. The experimental and simulated results showed close agreement. Compared with the rise time of the gripping force and the time for which the trigger was actually On, the time delay was calculated as 0.2 s. To provide a constant pressure, compressor's power was set as auto-compressed mode that kept the pressure inside of the tank.

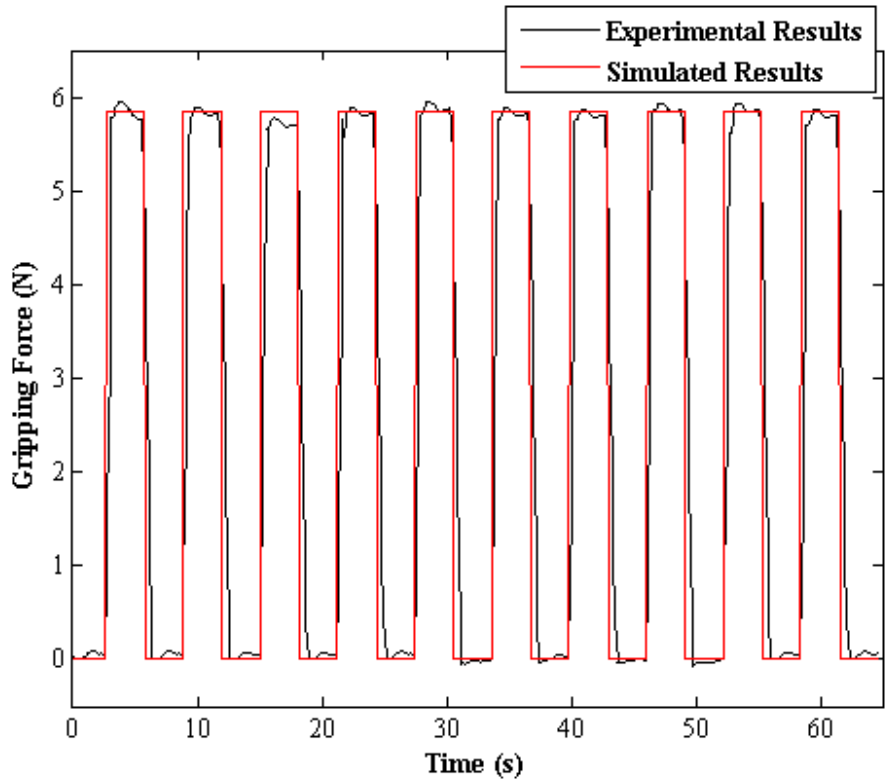

Fig. 3.3 Experimental results versus simulated results. The step function of the simulated result was similar to Fig. 3.2's experimental result for the gripping force at a pressure of 0.3 MPa.

3.2.1.4. Durability Test

For checking the durability of gripping system, the automatic trigger repeating algorithm was performed by repeating On/Off every specific second for 1,000 gripping motions. This experiment was also conducted at the representative value of 0.3 MPa for the same reason of the reaction time experiment. Table 3.3 presents the results of this experiment. The repeating experimental value was 5.8 N (SD: 0.2 N) compared with the reference value of 5.8 N (SD: 0.3 N). This result was within the standard deviation. In addition, the standard deviation of the repeating value decreased significantly compared to the reference value because of 1,000 repetitions.

Table 3.3 Repeated gripping experiment at pressure of 0.3 MPa

	Mean (N)	Standard deviation (N)
Reference value (from Equ. (3.2))	5.8	0. 3
1,000 times repeated value	5.8	0.2

3.2.2. Simple Peg Task

To evaluate the proposed surgical robot system, a block transfer task was performed as shown in Fig. 3.4. This task was achieved using the Fundamentals of Laparoscopic Surgery (FLS) peg transfer kit. The simple peg tasks were intended to measure the surgeon's technical skills and eye-hand coordination during basic laparoscopic surgery and to validate the surgical robot system's performance [26, 64]. These research followed the FLS curriculum alike our experiment and the time limit was set at 300 s [26, 64, 65]. FLS curriculum is: i) five novice volunteers were recruited for the experiment using the surgical instrument, ii) these volunteers were asked to lift six objects on the left side of the board and to transfer these object to the right side of the board, iii) the time for the peg task began when the volunteer grasped the first peg and ended upon the release of the last peg. These volunteers repeatedly performed three trials.

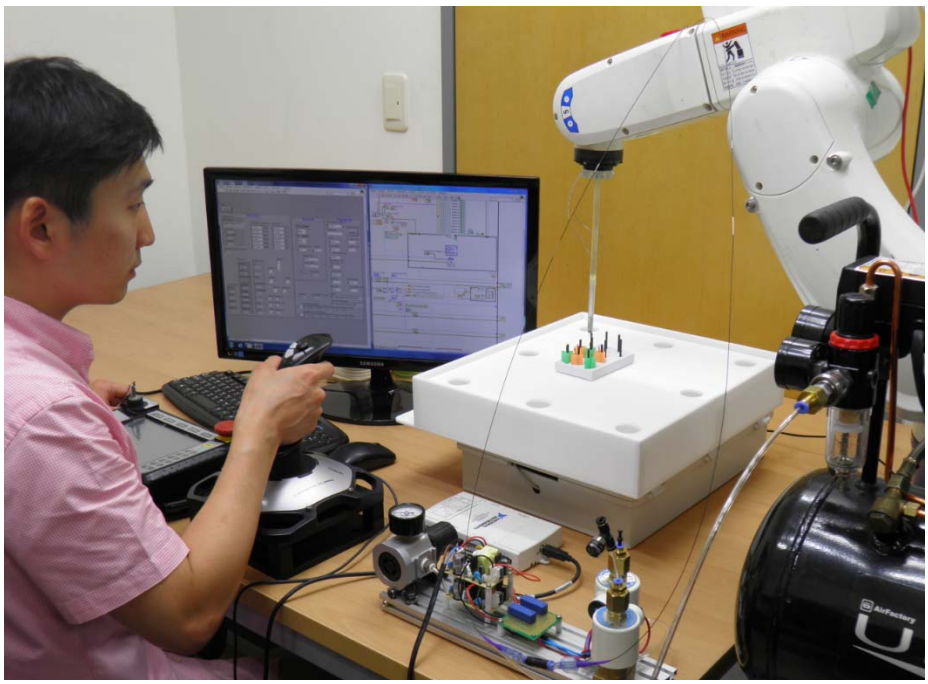

Fig. 3.4 Block transfer task. Peg task performed using Fundamental of Laparoscopic Surgery (FLS) task.

According to Table 3.4, the mean time for the peg task was 176 s. No one exceeded the cut-off time of 300 s in all trials. These results were found to be slightly long in comparison with the results using da Vinci research kit (dVRK), donated by Intuitive Surgical Inc. [66]. For same experimental environment, only one Master Tool Manipulator (MTM) and one Patient Side Manipulator (PSM) of dVRK were used. In the same curriculum for FLS, same volunteers were recruited to carry out the same task. Although amount of reduction time differed from volunteer to volunteer, the peg task's execution time of 48 ~ 81 s was decreased when it compared with the proposed system's results. The

standard deviation was smaller and more uniform than the proposed system's results. The volunteer 3 dropped the peg during the task which resulted in creating larger workspace and extra-long execution time. Except for this case, other volunteers showed better performance as they adapted to the system.

Table 3.4 Execution time of block transfer task

	Trial Number	Volunteer 1	Volunteer 2	Volunteer 3	Volunteer 4	Volunteer 5	Total Mean
SOBW	1	255	222	172	154	241	209
	2	221	192	115	153	174	171
	3	148	169	125	122	181	149
	Mean	208	194	137	143	199	176
	SD	45	22	25	15	30	27
dVRK	1	148	132	73	90	147	118
	2	167	108	66	98	131	114
	3	97	100	129	84	126	107
	Mean	137	113	89	91	135	113
	SD	30	14	28	6	9	4

* Abbreviation: Surgical-Operation-By-Wire (SOBW), Standard Deviation (SD), and da Vinci Research Kit (dVRK).

3.2.3. Workspace

Fig. 3.5 shows the calculated workspace. The workspace requirements for a robotic-assisted cholecystectomy were used to validate the proposed surgical robot system [67]. The driving range of each joint was considered using D-H parameters of the proposed system and surgical instrument's information as shown in Table 2.2 and Fig. 2.10. The workspace of entire joints satisfied more than 100% of the requirements for cholecystectomy. The workspace was calculated as 11,157.0 cm^3 which surpassed the 549.5 cm^3 of the reference's result [67].

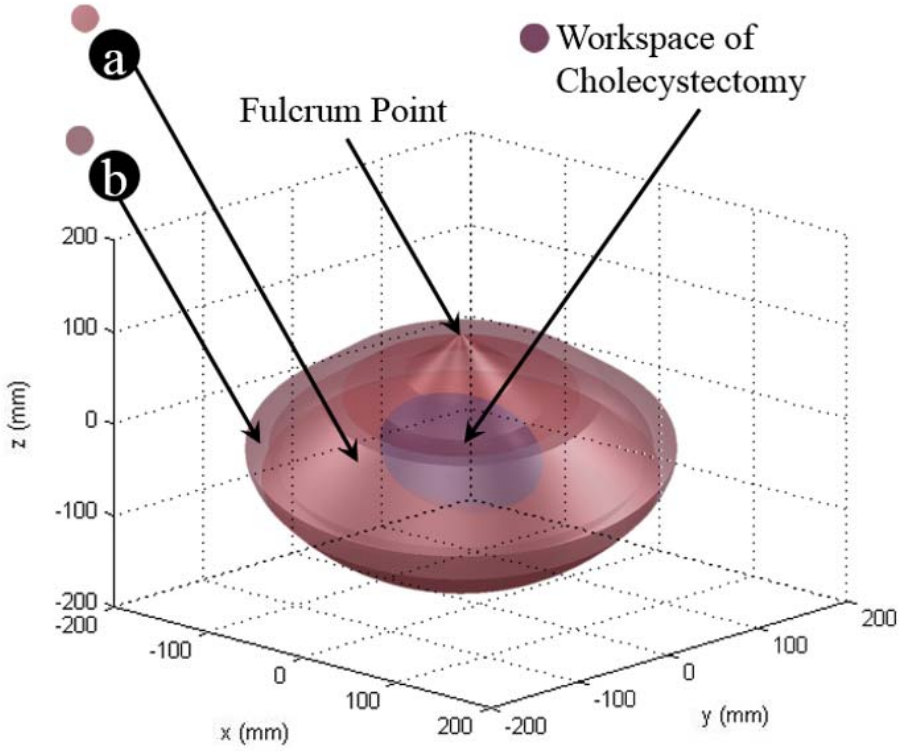

Fig. 3.5 Workspace of the proposed surgical robot system. (a) Elbow joint (J7) was considered with external arm (J1-J6). (b) Elbow and wrist joints (J7 and J8) were considered with external arm (J1-J6).

3.2.4. System Specification

Table 3.5 summarizes proposed surgical robot system that consists of surgical instrument (KS-4), external arm, master interface, and pneumatic system.

Table 3.5 System specifications of Surgical-Operation-By-Wire (SOBW)

Specification item	Unit		
Installing posture			Floor mounted
Construction			Vertical articulated type
Degree of freedom			9
Drive method		J1 ~ J6	AC servomotor
		J7 ~ J8	Brushless DC motor
		Gripper	Pneumatic
Arm length	mm		565 (external arm) + 300 (surgical instrument) = 865
Operation range	°	J1	±170
		J2	+135, -100
		J3	+166, -119
		J4	±190
		J5	±120
		J6	±360
		J7	±18
		J8	±30
Maximum speed	mm/s	J1 ~ J6	8,200
	rpm	J7 ~ J8	106
Weight	kg		35.036
Position repeatability	mm	J1 ~ J6	±0.02
Compressor's pressure range	MPa		0 ~ 0.8
Gripper's gripping force	N		0 ~ 9.96
Gripper's reaction time	s		0.2
Entire system's workspace	cm^2		11,157
Master interface			improved Hands-On-Throttle-And-Stick (iHOTAS, integrated with 6-axis force torque sensor)
Motion scaling range	%		0 ~ 200
Gripper functions			Gripping only
Sterilization			Not available

The proposed surgical robot system's gripper was able to perform the gripping motion only. In other words, it could not execute the coagulation function since our research is focused on development of the SOBW system. This system will function as forceps, scissor, and so on.

4. Discussion

Robotic surgery, an attractive alternative to conventional open and laparoscopic surgery, has been in clinical practice for many years. However, the lack of haptic feedback in current robotic systems was considered to be a limitation that prevented the surgeon from obtaining the sensory information that is desired for enhanced control of the robotic system. Without effective haptic feedback, a surgeon should perform the robotic surgery depending on visual cues and learn by cumulative cases to estimate the force and tension that is placed on tissues and sutures during the surgery. Estimation of the gripping forces of the robotic instruments carries clinical significance in this respect.

Mucksavage et al. measured the gripping forces of robotic instruments using a 2.2 mm button style compression load cell transducer and a training instrument [21]. These researchers reported that significant differences in the gripping force existed between the major deflections compared with the neutral and minor deflections in extended use training instruments. Minor deflections (movements along the distal wrist joint, yawing movements) and the neutral position exhibited a similar gripping force, whereas major deflections (movements at the proximal wrist joint, pitching movements) resulted in a significantly lower gripping force. It was examined the gripping force of the instruments at various angles of EndoWrist's roll, pitch, and yaw orientations,

which are afforded by the seven degrees of freedom. The gripping forces were measured for 27 different postures, to predict a quantitative compensation force for the da Vinci end-effector. Table 1.3 shows that the several gripping forces for different postures were different from the overall mean by a minimum of triple the amount. This result was observed when the two postures (14.15 N in A(90˚, 70˚, -90˚) and 4.20 N in A(-90˚, 70˚, 90˚)) of the P.D.F. EndoWrist were compared. This result implies that the additional force, 9.95 N, was required for the posture A(-90˚, 70˚, 90˚), which should be the compensation force for a reliable surgical operation. If gripping motion trigger (button #1 and #2) combines with pressure sensors to sense the surgeon's intention, EIMM will be modeled for both soft gripping mode and firm gripping mode.

In Table 1.3, three EndoWrists' Cronbach's alpha values were greater than, or equal, to the value of 0.99. This meant that the proposed gripping force measurement result had an excellent internal consistency [41]. In addition, EIMM was established using the quantitative results. Using EIMM at any posture, a calculation of the compensation force for a reliable surgical operation will be predictable.

To evaluate the linear model proposed in Equation (2.2), the errors for the linear model and the quadratic model were computed and compared for the P.F. EndoWrist, and those were 10.69% and 9.17%, respectively. Analysis using the higher degree polynomials term could not reduce the EIMM's prediction error significantly because of the mechanical and nonlinear characteristics of EndoWrist. This observation implies that the linear model proposed in this

research is adequate for the analysis. Although the least square method has an advantage of short calculation time, the prediction error was higher than the error of linear model (Equ. (2.3)).

Although the proposed optimal coefficient sets did not cover all the ranges of EndoWrist, it could be known which element among the Euler angles created excessive or less force to the EndoWrist. The P.F. EndoWrist was more affected by the roll and pitch movement of the joint than the yaw. The absolute value of C_α and C_β were greater than C_γ. A surgeon who uses P.F. EndoWrist should acknowledge that the roll and pitch movement will exceed or loosen the tissue traction. Especially P.D.F. EndoWrist users should pay attention to the roll movements. The L.N.D. EndoWrist was less sensitive to the change in the joint angle compared with the other EndoWrists.

P.F. EndoWrist exerted a maximum gripping force of 20.33 N in A(0˚, 0˚, -90˚), as shown in Table 1.3. In this posture, approximately 3.50 N (3.65 N and 3.31 N) and 4.50 N (4.07 N and 4.92 N) of the gripping force was loosened by changing into a roll movement of 0˚ to -90˚ or 0˚ to 90˚ and a yaw movement of -90˚ to 0˚ or -90˚ to 90˚, respectively. Specifically, almost half of the gripping force, 9.00 N (9.28 N and 8.71 N) was lost because of the posture changing the pitch angles 0˚ to -70˚ or 0˚ to 70˚. In contrast, 5.50 N (8.10 N and 2.89 N), 4.93 N (9.28 N and 0.57 N), and 2.37 N (2.16 N and 2.58 N) of the excessive gripping force were applied to EndoWrist while changing from the posture A(0˚, 70˚, -90˚) to any direction of moving into roll, pitch, and yaw movements. Based on these results, when moving a specific posture to movements of roll,

pitch, and yaw, a surgeon should pay special attention to avoid potential damage to tissue. In contrast to the above statement, to avoid a tissue slip incident using EndoWrist, the EndoWrist should be in a reinforced posture, to grab the tissue securely. If the gripping forces and the postures were measured and modeled with additional angles based on the EIMM, then the compensation force for any change of angles will be predictable.

Each EndoWrist had a varying set of optimal coefficients and errors for the model because of the tensions on the mechanical strings for gripping motion of EndoWrists were depend on which EndoWrist was used since every EndoWrist's design, mechanism, string interferences, and the EndoWrist's special function, components, and lifespan were subtly different for its own usage. However, because the standard deviations were significantly small and the values of Cronbach's alpha were estimated as close to the value of 1, gripping force results and coefficient using EIMM could be consider to be sufficient to verify that evaluation of the methodology and interpretation of the result were acceptable in this research. To reduce modeling errors, additional combinations of EndoWrist's posture, coupled terms, and lifespan could be considered.

The potential limitations of this research should be addressed as a means for improvement or for mapping out strategies for future study. Knowledge of these differences in the gripping force might be unlikely to have any major clinical significance. However, there might be interpersonal variations among learning curves of different surgeons based on their skills and experiences.

Understanding the mechanical properties of the robotic system is important to ensure the safe implementation of robotic surgery for less experienced surgeons. The proposed model for EndoWrists had several positive and significant benefits: i) surgeon was able to realize the compensation gripping force by EIMM for varying postures ii) if novel torque transfer system using AC servo motor with EIMM were developed, surgeon does not have to consider non-uniform gripping force on laparoscopic robotic surgery because the torque transfer system would calculate the compensation gripping force and compensate the gripping force by exerting torque control iii) continuous calibration using EIMM will resolve the mechanical string's tension issue without any change on EndoWrist's design and mechanism iv) This will greatly increase the safety of the operation procedure.

The developed TTS (KS-2) in this research was different from the da Vinci robot arm's torque transfer system. However, the gripping force comparison between the proposed measurement using TTS in this research and actual da Vinci system's results [21] showed an accordant tendency and the gripping forces of three postures ((0˚, 0˚, 0˚), (0˚, 0˚, 90˚), and (0˚, 0˚, -90˚)) were also comparable with the actual da Vinci system's results. The amount of values of gripping force for the two postures ((0˚, 70˚, 0˚) and (0˚, -70˚, 0˚)), which were related to up/down motions, were somewhat different. This was caused by the amount of the differences for deflections between our experiment setup and the experiment using actual da Vinci system [21]. The amount of deflections about right/left movements of EndoWrist was similar, while it was different for the

up/down movements. Although the experimental set-up was unidentical to the real surgical operation, the proposed model and the results from this research are highly valuable because they provide a gripping force analysis and because they predict the grip compensation force without measuring the forces applied to the organs, vessels, or other tissue. The technique also provides the basis for haptic force feedback modeling and is applicable to other end-effectors, especially scissors, because their shapes and structures are notably similar.

The gripping force predictive linear equations (3.2) and (3.3) could provide the gripping force for the pressure range of 1 to 0.775 MPa with 0.025 MPa intervals. The slope of equation (3.2), c_1 was greater than the slope of equation (3.3), c_2. Two sections were used owing to air saturation of the catheter balloon. Limited to the diameter of the catheter balloon, it was difficult to generate a greater force for a pressure of 0.35 MPa. The proposed gripping system is remarkable in terms of its decoupling with other joint movements. The value of the gripping force was in close agreement with those of numerous studies [28, 68, 69]. It is expected that greater gripping force will be generated at higher pressures.

According to Fig. 3.3, the experimental and ideal simulated results showed good agreement. The time delay of 0.2 s occurred in passing the pneumatic system, consisting of the SVs, pressure/speed controller, and pneumatic tubes. To reduce the reaction time, length of tube was minimized. Time delay effect (without delay vs. 0.25 s delay) did not affect the task completion time significantly for simple peg task using FLS similar to our research (subjects:

non-surgeon) [70]. Furthermore, Sandor Jordan et al. reported that human could adapt to an amount of time delay in robotic surgery, typically maximum of 0.5 s [71]. This means that the pneumatic gripping system reacts to the surgeon's intention in acceptable time delay of 0.2 s, enabling almost real-time control.

A repeated gripping experiment indicated the durability of the surgical robot's instrument. Despite 1,000 repetitions, the gripping force was not affected. This result addressed that surgical instrument's gripper was greatly durable for many open/close cycles. Although the proposed gripper was not directly compared with da Vinci's EndoWrist which needed to be discarded after 5 ~ 10 surgeries, it could present a new approach to the next-generation surgical robot's end-effector for cost effective and reliable surgery. However, like a da Vinci EndoWrist, the successful development of the proposed surgical robot's gripper should consider sterility issue. Thus, modifying the proposed gripper with the outer shell made of stainless steel and studying the sealing issue are planned in the future.

The simple peg task results were fairly short in comparison to those of other similar studies using same FLS curriculum and FLS kit [26, 64]. It is inferred that the proposed surgical robot system shows good performance and effectiveness for laparoscopic surgery. Most of the results were shorter than those of previous trials. This means that the novice volunteers quickly adapted to the surgical robot system and showed different performances depending on their ability. However, mean of peg task's execution time and standard deviation were slightly longer compared with the results using dVRK. The

major cause of these results was the slow moving velocity of external arm and surgical instrument (KS-4). This could be overcome by the improvement of the proposed system's stable control in high speed.

The trajectory of the proposed surgical robot system made a cone shape around a fulcrum point as shown in Fig. 3.5. The status of straight surgical instrument's reachable workspace (not bended by elbow and wrist joints) was extended by translational movement of external arm. The region of the Fig. 3.5-(a) and (b) were calculated by considering elbow joint movement and elbow & wrist movement, respectively. The proposed surgical robot system would be applicable to other many surgeries covering the cholecystectomy because of its larger workspace. It is even possible to obtain much larger workspace than the current workspace when expanding the movable range of predefined external arm's limits.

The iHOTAS controller with a 6-axis force/torque sensor sensed the surgeon's intention of translational movement. It could help in developing a force feedback system. The 6-axis force/torque sensor information, being recorded in real-time, could be analyzed to determine the intent of the surgeon.

Based on the improved feature of the proposed system, SOBW concept, iHOTAS control interface, and novel pneumatic gripping system could be a substitution for other previous surgical robot system developed using mechanical strings and other mechanical parts.

Despite the proposed surgical robot system's applicability, some improvements are needed. It contains some fragile parts because it was manufactured using a 3-D printer's synthetic resins. To ensure reliability, the prototype surgical instrument should be manufactured using solid materials. In addition, the proposed surgical instrument should resolve sterility issue. Thus, modifying the surgical instrument with the outer shell made of stainless steel and studying the sealing issue will be needed in the future. Then, clinical issues are planned to be considered as a future study, too. Furthermore, a force feedback system should be added using an iHOTAS controller with force sensors.

5. Conclusion

The number of surgical operations performed with da Vinci has been rapidly increasing because it has many benefits. However, different gripping force for different postures is currently applied, while the surgeon does not recognize the different forces. This issue could lead to a serious accident.

In this research, a TTS (KS-2) has been developed to measure the EndoWrist gripping forces. It was observed that the measured gripping forces for the two different postures differed by 3.37 times (14.15 N vs. 4.20 N). This result means that a compensation force will be required for a safe and reliable operation. To predict the compensation force, a linear mathematical model of EndoWrist's inner mechanism has been developed, and the model has been validated by comparing the expected gripping force from the model with the measured gripping force from the da Vinci. To apply EIMM to laparoscopic robotic surgery, the automatic calibration procedure would be needed.

A surgical instrument (KS-4) with a pneumatic gripping system and pitching/yawing joints using micro motors was developed for SOBW. This instrument was used to perform a simple peg task with a 6-axis external arm by surgeon's control using an iHOTAS controller. A gripping force measurement experiment and block transfer task were conducted. To evaluate the proposed system's clinical applicability, the workspace was calculated. Based on these results, the proposed system is expected to be widely used for laparoscopic robotic surgery.

References

[1] Kang BH, Xuan Y, Hur H, Ahn CW, Cho YK, Han S-U: **Comparison of Surgical Outcomes between Robotic and Laparoscopic Gastrectomy for Gastric Cancer: The Learning Curve of Robotic Surgery.** *J Gastric Cancer* 2012, **12**(3):156-163.

[2] Sung GT, Gill IS: **Robotic laparoscopic surgery: a comparison of the da Vinci and Zeus systems.** *Urology* 2001, **58**(6):893-898.

[3] Corcione F, Esposito C, Cuccurullo D, Settembre A, Miranda N, Amato F, Pirozzi F, Caiazzo P: **Advantages and limits of robot-assisted laparoscopic surgery: preliminary experience.** *Surgical endoscopy* 2005, **19**(1):117-119.

[4] Lanfranco AR, Castellanos AE, Desai JP, Meyers WC: **Robotic surgery: a current perspective.** *Annals of surgery* 2004, **239**(1):14-21.

[5] Hannaford B, Rosen J, Friedman DW, King H, Roan P, Cheng L, Glozman D, Ma J, Kosari SN, White L: **Raven-II: an open platform for surgical robotics research.** *IEEE transactions on bio-medical engineering* 2013, **60**(4):954-959.

[6] Heemskerk J, Bouvy ND, Baeten CG: **The end of robot-assisted laparoscopy? A critical appraisal of scientific evidence on the use of robot-assisted laparoscopic surgery.** *Surgical endoscopy* 2014, **28**(4):1388-1398.

[7] Howe RD, Matsuoka Y: **Robotics for surgery.** *Annual review of biomedical engineering* 1999, **1**:211-240.

[8] Kwoh YS, Hou J, Jonckheere EA, Hayati S: **A Robot with Improved Absolute Positioning Accuracy for CT Guided Stereotactic Brain Surgery.** *IEEE transactions on bio-medical engineering* 1988, **35**(2):153-160.

[9] Satava RM: **Surgical robotics: The early chronicles - A personal historical perspective.** *Surg Laparo Endo Per* 2002, **12**(1):6-16.

[10] Pransky J: **ROBODOC - Surgical robot success story.** *Ind Robot* 1997, **24**(3):231-233.

[11] Kraft BM, Jager C, Kraft K, Leibl BJ, Bittner R: **The AESOP robot system in laparoseopic surgery - Increased risk or advantage for surgeon and patient?** *Surgical Endoscopy and Other Interventional Techniques* 2004, **18**(8):1216-1223.

[12] **INTUITIVE SURGICAL AND COMPUTER MOTION ANNOUNCE MERGER AGREEMENT** [http://sec.edgar-online.com/intuitive-surgical-inc/8-k-current-report-filing/2003/03/07/Section10.aspx]

[13] **A Brief History of Robotic Surgery** [http://hoffroboticsurgery.com/roboticsurgery.html]

[14] **Robotics: the Future of Minimally Invasive Heart Surgery** [http://biomed.brown.edu/Courses/BI108/BI108_2000_Groups/Heart_Surgery/Robotics.html]

[15] **NEEMO 7: NASA'S Undersea Robotic Telemedicine Experiment**

[http://www.space.com/445-neemo-7-nasa-undersea-robotic-telemedicine-experiment.html]

[16] **The da vinci surgery experience: over the past decade, more than 1.5 million surgeries have been performed worldwide using the da Vinci Surgical System** [http://www.davincisurgery.com/assets/docs/da-vinci-surgery-fact-sheet-en-1005195.pdf?location=1&version=b]

[17] **Tracking the Rise of Robotic Surgery for Prostate Cancer** [http://www.cancer.gov/about-cancer/treatment/research/rise-robotic-surgery]

[18] **da Vinci Surgical Robot Complaints on the Rise; Lawsuits Begin** [http://olsmanlaw.com/main/da-vinci-surgical-robot-complaints-on-the-rise-lawsuits-begin/]

[19] **Cardiac Surgery in the Age of IT** [http://www.medicaldevice-network.com/features/feature106713/feature106713-3.html]

[20] Hashizume M, Konishi K, Tsutsumi N, Yamaguchi S, Shimabukuro R: **A new era of robotic computer-enhanced surgery assisted by a surgical system.** *Surgery* 2002, **131**(1):330-333.

[21] Mucksavage P, Kerbl DC, Pick DL, Lee JY, McDougall EM, Louie MK: **Differences in Grip Forces Among Various Robotic Instruments and da Vinci Surgical Platforms.** *J Endourol* 2011, **25**(3):523-528.

[22] Tavakoli M, Patel RV, Moallem M: **Haptic interaction in robot-assisted endoscopic surgery: a sensorized end-effector.** *Int J Med Robot Comp* 2005, **1**(2):53-63.

[23] King CH, Culjat MO, Franco ML, Lewis CE, Dutson EP, Grundfest WS, Bisley JW: **Tactile Feedback Induces Reduced Grasping Force in Robot-Assisted Surgery.** *IEEE T Haptics* 2009, **2**(2):103-110.

[24] Park SY, Cho KS, Lee SW, Soh BH, Rha KH: **Intraoperative breakage of needle driver jaw during robotic-assisted laparoscopic radical prostatectomy.** *Urology* 2008, **71**(1):168.

[25] Dobbelsteen JJ, Lee RA, Noorden M, Dankelman J: **Indirect measurement of pinch and pull forces at the shaft of laparoscopic graspers.** *Med Biol Eng Comput* 2012, **50**(3):215-221.

[26] Shin WH, Kwon DS: **Surgical robot system for single-port surgery with novel joint mechanism.** *IEEE transactions on bio-medical engineering* 2013, **60**(4):937-944.

[27] Jienan D, Kai X, Goldman R, Allen P, Fowler D, Simaan N: **Design, simulation and evaluation of kinematic alternatives for Insertable Robotic Effectors Platforms in Single Port Access Surgery.** In *Robotics and Automation (ICRA), 2010 IEEE International Conference on*; *3-7 May 2010*. 2010:1053-1058.

[28] Quaglia C, Petroni G, Niccolini M, Caccavaro S, Dario P, Menciassi A: **Design of a Compact Robotic Manipulator for Single-Port Laparoscopy.** *Journal of Mechanical Design* 2014, **136**(10):871-878.

[29] Sun Z, Ang RY, Lim EW, Wang Z, Ho KY, Phee SJ: **Enhancement of a master-slave robotic system for natural orifice transluminal endoscopic surgery.** *Annals of the Academy of Medicine, Singapore* 2011, **40**(5):223-230.

[30] Simorov A, Otte RS, Kopietz CM, Oleynikov D: **Review of surgical robotics user interface: what is the best way to control robotic surgery?** *Surgical Endoscopy and Other Interventional Techniques* 2012, **26**(8):2117-2125.

[31] Hagn U, Konietschke R, Tobergte A, Nickl M, Jorg S, Kubler B, Passig G, Groger M, Frohlich F, Seibold U, et al: **DLR MiroSurge: a versatile system for research in endoscopic telesurgery.** *Int J Comput Ass Rad* 2010, **5**(2):183-193.

[32] Lum MJH, Friedman DCW, Sankaranarayanan G, King H, Fodero K, Leuschke R, Hannaford B, Rosen J, Sinanan MN: **The RAVEN: Design and Validation of a Telesurgery System.** *Int J Robot Res* 2009, **28**(9):1183-1197.

[33] Sutherland GR, Wolfsberger S, Lama S, Zarei-nia K: **The Evolution of neuroArm.** *Neurosurgery* 2013, **72**:27-32.

[34] Seibold U, Kubler B, Hirzinger G: **Prototype of Instrument for Minimally Invasive Surgery with 6-Axis Force Sensing Capability.** In *Robotics and Automation, 2005 ICRA 2005 Proceedings of the 2005 IEEE International Conference on*; *18-22 April 2005*. 2005:496-501.

[35] Greenish S, Hayward V, Chial V, Okamura A, Steffen T: **Measurement, analysis, and display of haptic signals during surgical cutting.** *Presence-Teleop Virt* 2002, **11**(6):626-651.

[36] **Application Note Medical Technology: Surgical Robots for Minimally Invasive Procedures**

[http://www.maxonmotor.com/medias/sys_master/8798145740830/O

P-Robot-en.pdf?attachment=true]

[37] **maxon DC motor** [http://www.engr.ucsb.edu/~mdnip/me170c/datasheets/25mm_Motors.pdf]

[38] Mosse CA, Mills TN, Bell GD, Swain CP: **Device for measuring the forces exerted on the shaft of an endoscope during colonoscopy.** *Med Biol Eng Comput* 1998, **36**(2):186-190.

[39] Boissy P, Bourbonnais D, Carlotti MM, Gravel D, Arsenault BA: **Maximal grip force in chronic stroke subjects and its relationship to global upper extremity function.** *Clin Rehabil* 1999, **13**(4):354-362.

[40] American Educational Research Association APA, National Council on Measurement in Education: **Standard for educational and psychological testing.** Washington, DC: American Psychological Association; 2014.

[41] George D, Mallery P: **SPSS for Windows Step by Step: A Simple Guide and Reference, 13.0 Update.** Pearson A and B; 2006.

[42] Johnson PJ, Schmidt DE, Duvvuri U: **Output control of da Vinci surgical system's surgical graspers.** *Journal of Surgical Research* 2014, **186**(1):56-62.

[43] Millard DJ: **Fly by Wire Control-System.** *Aircraft Eng* 1972, **44**(8):4.

[44] Burns BRA: **Fly-by-Wire and Control Configured Vehicles - Rewards and Risks.** *Aeronaut J* 1975, **79**(770):51-58.

[45] **From cable controlled flight controls to FBW** [http://asn-

xp.aerosoft.com/?page_id=3826]

[46] Collinson RPG: **Fly-by-Wire Flight Control.** *Aircraft Eng* 1978, **50**(2):8-13.

[47] Dugan JB, Vanburen R: **Reliability Evaluation of Fly-by-Wire Computer-Systems.** *J Syst Software* 1994, **25**(1):109-120.

[48] Andrade L, Tenning C: **Design of the Boeing 777 electric system.** In *Aerospace and Electronics Conference, 1992 NAECON 1992, Proceedings of the IEEE 1992 National*; *18-22 May 1992*. 1992:1281-1290.

[49] Sungwan Kim, 김유단, 김현회, 김희찬, 박용현, 이치원, 김원식, 윤치열, 노승우, 이충희: **SOBW형 수술 장치.** In. 대한민국; 2013. [Vol. 10-2013-0134162].

[50] Sungwan Kim, Youdan Kim, Hyeon Hoe Kim, Hee Chan Kim, Yong Hyun Park, Chiwon Lee, Wonshik Kim, Chiyul Yoon, Seungwoo Noh, Choonghee Lee: **Surgical-Operation-By-Wire Type Surgical Operation Apparatus.** In. US; 2013.[Vol. 14/078,395].

[51] Wortman TD, Mondry JM, Farritor SM, Oleynikov D: **Single-site colectomy with miniature in vivo robotic platform.** *IEEE transactions on bio-medical engineering* 2013, **60**(4):926-929.

[52] Lassooij J, Tolou N, Tortora G, Caccavaro S, Menciassi A, Herder JL: **A statically balanced and bi-stable compliant end effector combined with a laparoscopic 2DoF robotic arm.** *Mech Sci* 2012, **3**(2):85-93.

[53] Zhao BL, Nelson CA: **A Cable-Driven Grasper with Decoupled**

Motion and Forces. *J Med Devices* 2014, **8**(3):1-2.

[54] Gijsen FJH, Migliavacca F, Schievano S, Socci L, Petrini L, Thury A, Wentzel JJ, van der Steen AFW, Serruys PWS, Dubini G: **Simulation of stent deployment in a realistic human coronary artery.** *Biomed Eng Online* 2008, **7**(23):1-11.

[55] Sungwan Kim, 김유단, 김현회, 김희찬, 박용현, 이치원, 김원식, 윤치열, 노승우, 이충희: **전동 수술 기구.** In. 대한민국; 2013. [Vol. 10-2013-0020379].

[56] Sungwan Kim, 김유단, 김현회, 김희찬, 박찬국, 이충희, 이치원, 박용현, 노승우, 윤치열: **외과 수술 로봇 조작 장치.** In. 대한민국; 2011. [Vol. 10-2011-0109426].

[57] Sungwan Kim, Youdan Kim, Hyeon Hoe Kim, Hee Chan Kim, Chan GookPark, Choonghee Lee, Chiwon Lee, Yong Hyun Park, Seungwoo Noh, Chiyul Yoon: **Control Apparatus for Surgical Robot.** In. US; 2012. [Vol. 13/585,246].

[58] Abbott DJ, Becke C, Rothstein RI, Peine WJ: **Design of an endoluminal NOTES robotic system.** In *Intelligent Robots and Systems, 2007 IROS 2007 IEEE/RSJ International Conference on*; *Oct. 29 2007-Nov. 2 2007*. 2007:410-416.

[59] Kuebler B, Seibold U, Hirzinger G: **Development of actuated and sensor integrated forceps for minimally invasive robotic surgery.** *Int J Med Robot Comp* 2005, **1**(3):96-107.

[60] Serdar Kucuk ZB: **Robot Kinematics: Forward and Inverse**

Kinematics. In *Industrial Robotics: Theory, Modeling and Control.* Edited by Cubero S. ARS, Austria Pro Literatur Verlag; 2006: 964.

[61] Gupta GS, Mukhopadhyay SC, Messom CH, Demidenko SN: **Master-slave control of a teleoperated anthropomorphic robotic arm with gripping force sensing.** *IEEE T Instrum Meas* 2006, **55**(6):2136-2145.

[62] Bromba MUA, Ziegler H: **Application Hints for Savitzky-Golay Digital Smoothing Filters.** *Anal Chem* 1981, **53**(11):1583-1586.

[63] Candan C, Inan H: **A unified framework for derivation and implementation of Savitzky-Golay filters.** *Signal Process* 2014, **104**:203-211.

[64] Joseph RA, Goh AC, Cuevas SP, Donovan MA, Kauffman MG, Salas NA, Miles B, Bass BL, Dunkin BJ: **"Chopstick" surgery: a novel technique improves surgeon performance and eliminates arm collision in robotic single-incision laparoscopic surgery.** *Surgical Endoscopy and Other Interventional Techniques* 2010, **24**(6):1331-1335.

[65] Dulan G, Rege RV, Hogg DC, Gilberg-Fisher KM, Arain NA, Tesfay ST, Scott DJ: **Developing a comprehensive, proficiency-based training program for robotic surgery.** *Surgery* 2012, **152**(3):477-488.

[66] **Welcome to the da Vinci Research Kit wiki community** [http://research.intusurg.com/dvrkwiki/index.php?title=Main_Page]

[67] Dongchun L, Jinhua L, Chao H, Kang K: **Workspace analysis based port placement planning in robotic-assisted cholecystectomy.** In *IT in Medicine and Education (ITME), 2011 International Symposium on*;

9-11 Dec. 2011. 2011:616-620.

[68] Gupta V, Reddy NP, Batur P: **Forces in surgical tools: comparison between laparoscopic and surgical forceps.** In *Engineering in Medicine and Biology Society, 1996 Bridging Disciplines for Biomedicine Proceedings of the 18th Annual International Conference of the IEEE*; *31 Oct-3 Nov 1996*. 1996:223-224.

[69] Sukthankar SM, Reddy NP: **Towards force feedback in laparoscopic surgical tools.** In *Engineering in Medicine and Biology Society, 1994 Engineering Advances: New Opportunities for Biomedical Engineers Proceedings of the 16th Annual International Conference of the IEEE*; *1994*. 1994:1041-1042.

[70] Lum MJ, Rosen J, King H, Friedman DC, Lendvay TS, Wright AS, Sinanan MN, Hannaford B: **Teleoperation in surgical robotics--network latency effects on surgical performance.** *Conference proceedings: Annual International Conference of the IEEE Engineering in Medicine and Biology Society IEEE Engineering in Medicine and Biology Society Annual Conference* 2009, 2009:6860-6863.

[71] **Modelling and Control Framework for Robotic Telesurgery** [http://www.cascade-fp7.eu/cras2013/proceedings/cras2013_Jordan.pdf]

국문초록

기존의 개복 수술에 비해 최소 침습 수술은 많은 장점이 있다. 하지만 기존 복강경 도구를 이용한 최소 침습 수술의 한계를 극복하고자 로봇을 이용한 복강경 수술이 널리 시행되고 있다. 하지만 대표적인 복강경 수술 로봇인 다빈치 로봇의 경우 엔드이펙터의 집게가 다양한 자세에서 균일한 힘을 내지 못하는 것이 다른 연구진에 의해 밝혀졌다. 본 연구에서는 이를 가설로 두고 이를 구체적인 실험으로 규명하였으며, 문제의 원인이 금속 줄로 제어되는 엔드이펙터 때문임을 증명하였다. 이를 위해 엔드이펙터의 집는 힘, 자세에 따른 커넥터 각도, 전달 토크를 새로이 고안한 토크전달시스템으로 측정하였다. 측정 결과 의사의 균일한 의도에도 불구하고 27가지 자세에서 세가지 엔드이펙터가 모두 다른 힘을 내었으며 최소 1.84배에서 최대 3.37배의 차이가 나는 것을 확인하였다.

이러한 단점을 극복하고자 본 연구에서는 두 가지 측면에서 해결책을 제시하였다.

첫째로, 다빈치의 엔드이펙터 내부 메커니즘을 분석하여 엔드이펙터의 다양한 자세에서 균일한 힘을 내기 위한 보상 힘을 제시하는 모델을 개발하였다. 모델에서 계산되는 값과 실제 값을 비교하여 검증하였다. 토크전달시스템을 통해 얻은 파라미터로부터 10.69-16.25%의 오차 범위 내에서 예측 집는 힘을 계산하는

결과를 도출하였다. 본 모델을 이용하면 기존 다빈치 시스템의 구조적 문제를 소프트웨어적으로 극복하는데 도움을 줄 수 있다. 또한 의사는 엔드이펙터 집게에 작용하는 실제 힘에 대한 정보를 얻을 수 있으며, 마스터 인터페이스에 압력 센서 등이 구비되면 집는 힘을 원하는 대로 조정할 수도 있어서 수술 도중 발생할 수 있는 사고를 미연에 방지 할 수 있다.

둘째로, 다빈치 시스템의 구조적 문제를 근본적으로 해결하기 위하여 새로운 수술 로봇 엔드이펙터 시스템, Surgical-Operation-By-Wire (SOBW)를 개발하였다. 6축 로봇팔을 사용하여 새로운 엔드이펙터와 함께 수술에 쓰일 수 있는 추가의 자유도를 갖추었다. 제안된 수술 로봇 시스템은 항공우주공학기술에 널리 쓰이는 Hands-On-Throttle-And-Stick (HOTAS)을 활용하여 6축 힘/토크 센서가 추가된 iHOTAS 인터페이스를 통해 제어된다. 집게의 반응시간이 0.2초로 계산되었고, 본 시스템을 처음 접하는 참가자가 술기 테스트에서 평균 176초안에 수행하여 300초 컷오프 타임안에 수행할 수 있게 시스템이 잘 구성되었음을 확인하였다. 또한 시스템의 동작 범위는 11,157.0 cm^3으로 계산되었다. 다양한 검증을 통해 제안된 수술 로봇 시스템이 실제 수술에 충분히 쓰일 수 있음을 확인하였다.

핵심어: 복강경 수술 로봇, 수술 로봇 엔드이펙터, 집는 힘 모델링, 전기신호식 수술 로봇 제어, 공압 집게.
학번: 2011-23432